Internal gravity waves versus inertial waves in the laboratory

Sylvain Joubaud, Samuel Boury, Philippe Odier

ACADÉMIE
DES SCIENCES
INSTITUT DE FRANCE

Comptes Rendus

Physique

Sylvain Joubaud, Samuel Boury and Philippe Odier

Internal gravity waves versus inertial waves in the laboratory

Published online: 7 November 2024

Part of Special Issue: Geophysical and astrophysical fluid dynamics in the laboratory
Guest editors: Stephan Fauve (Laboratoire de Physique de l'ENS, CNRS, PSL Research University, Sorbonne Université, Université Paris Cité, Paris, France) and Michael Le Bars (CNRS, Aix Marseille Univ, Centrale Marseille, IRPHE, Marseille, France)

https://doi.org/10.5802/crphys.197

The Comptes Rendus. Physique *are a member of the Mersenne Center for open scientific publishing*
www.centre-mersenne.org — e-ISSN : 1878-1535

ACADÉMIE DES SCIENCES
INSTITUT DE FRANCE

Comptes Rendus. Physique
Published online: 7 November 2024
https://doi.org/10.5802/crphys.197

Review article / *Article de synthèse*

Geophysical and astrophysical fluid dynamics in the laboratory / *Dynamique des fluides géophysiques et astrophysiques au laboratoire*

Internal gravity waves versus inertial waves in the laboratory

Ondes internes de gravité versus ondes inertielles au laboratoire

Sylvain Joubaud [*,a], **Samuel Boury** [b] **and Philippe Odier** [a]

[a] Ens de Lyon, CNRS, Laboratoire de Physique, Lyon, France

[b] Université Paris-Saclay, CNRS, FAST, 91405 Orsay, France

E-mails: sylvain.joubaud@ens-lyon.fr (S. Joubaud), samuel.boury@universite-paris-saclay.fr (S. Boury), philippe.odier@ens-lyon.fr (P. Odier)

Abstract. Density-stratified and/or rotating fluids are very common in geophysical and astrophysical flows and enable the propagation of respectively internal gravity waves and inertial waves. Their peculiar dispersion relation has the same mathematical form for both classes of waves and can lead to unexpected outcomes through amplification, resonance or non-linearities. Even though their dispersion relation is very similar, internal gravity waves and inertial waves have different structural characteristics and arise from distinct physical mechanisms. Understanding the analogies and the differences in their behaviors is crucial for studying their respective roles. In this review, we will describe laboratory experiments that have studied either inertial waves in rotating homogeneous fluids or internal gravity waves in non-rotating density stratified fluids to highlight both the similarities and the differences between these two types of waves. We will focus on linear and non-linear phenomena occurring for three different configurations: wave beams in 2D and in 3D geometry, axisymmetric waves, as well as wave attractors, a specific feature for these waves. In particular, we will describe the influence of these various configurations on the Triadic Resonant Instability (TRI).

Résumé. Les fluides stratifiés en densité et/ou tournants sont très courants dans les écoulements géophysiques et astrophysiques et permettent respectivement la propagation d'ondes internes de gravité et d'ondes inertielles. Mathématiquement, la relation de dispersion particulière a la même forme pour les deux classes d'ondes et peut conduire à des résultats inattendus via amplification, résonance ou non-linéarités. Même si leur relation de dispersion est très similaire, les ondes internes de gravité et les ondes d'inertie ont des caractéristiques structurelles différentes et résultent de mécanismes physiques distincts. Comprendre les analogies et les différences dans leurs dynamiques est crucial pour étudier leurs rôles respectifs. Dans cette revue, nous décrirons des expériences en laboratoire qui ont étudié soit les ondes d'inertie dans un fluide homogène en rotation, soit les ondes internes de gravité dans un fluide stratifié en densité non tournant, afin de mettre en évidence à la fois les similitudes et les divergences entre ces deux types d'ondes. Nous nous concentrerons sur les phénomènes linéaires et non linéaires se produisant pour trois configurations différentes : les

* Corresponding author

faisceaux d'ondes en géométrie 2D et 3D, les ondes axisymétriques, ainsi que les attracteurs d'ondes, spécificité de ces ondes. En particulier, nous décrirons l'influence de ces différentes configurations sur l'instabilité triadique résonante (TRI).

Keywords. Internal gravity waves, Inertial waves, Stratified fluid, Rotating fluid, Triadic Resonant Instability, wave attractors.

Mots-clés. Ondes internes de gravité, Ondes inertielles, Fluides stratifiés, Fluides en rotation, Instabilité par résonance triadique, attracteurs d'ondes.

Funding. The authors acknowledge support from the Simons Foundation through Grant No. 651475. S. Joubaud acknowledge the support from Institut Universitaire de France.

Manuscript received 19 April 2024, revised 23 July 2024, accepted 5 August 2024.

1. Introduction

Internal gravity waves and inertial waves are two distinct classes of waves that commonly occur in fluid dynamics, respectively for density stratified fluids and rotating fluids [1]. On the one hand, internal gravity waves correspond to disturbances in the density structure of the fluid, which leads to buoyancy forces acting as a restoring force. In a non-rotating density stratified fluid, the energy flux of pure monochromatic internal gravity waves propagates in a direction tilted by an angle β with the horizontal, given by the dispersion relation [2, 3]

$$\omega = N \sin\beta, \tag{1}$$

with N the buoyancy frequency, which characterizes the stratification of the fluid.
On the other hand, pure inertial waves result from the action of the Coriolis force leading to an energy flux for monochromatic waves also inclined by an angle β with the horizontal defined by the dispersion relation [4]

$$\omega = 2\Omega \cos\beta, \tag{2}$$

with Ω the solid rotation rate of the fluid. As a comparison to the vertical density stratification, Coriolis force in rotating flows leads to a horizontal stratification in angular momentum.

In various geophysical and astrophysical phenomena, the dynamics is often based on a coupling between rotation and gravity. Such flows are therefore dominated by inertia-gravity waves, which is a combination of internal gravity waves and inertial waves. This type of waves share similar properties since their dispersion relation explicitly involves a coupling between the two characteristic frequencies N and $f = 2\Omega$

$$\omega^2 = N^2 \sin^2\beta + f^2 \cos^2\beta\,. \tag{3}$$

Internal gravity waves and inertial waves are fundamental phenomena observed in various fluid systems, including the ocean, atmosphere, and astrophysical environments. In the oceans, these waves play a crucial role in mixing water masses, redistributing nutrients and heat, and influencing oceanic currents and circulation patterns [5–10]. Atmospheric internal waves often arise in stably stratified layers, such as within the troposphere or the bottom boundary layer, and contribute to turbulence, cloud formation, and the propagation of weather systems [10–14]. Gravity and inertial waves are also observed in astrophysical environments, such as stars, where they influence stellar dynamics, energy transport, and magnetic field generation [15–19].

The large scale of fluids in geophysical and astrophysical bodies induces for the waves a cascade of mechanical energy resulting from wave-wave, wave-vortex, wave-topography and/or wave-mean flow interactions. In particular, Triadic Resonant Instability (TRI) is an important type of wave-wave interaction that plays a major role in various geophysical contexts, and that has been extensively studied in the literature [20]. TRI is characterized by the non-linear

generation of two subharmonic secondary waves from a monochromatic primary wave, forming a triad of temporally and spatially resonant waves. We will come back throughout this article on various features of this instability. In general, these interactions result in an energy transfer from large scale to small scale structures so that waves can break and lead to turbulence and mixing or are dissipated through viscosity and diffusivity [21].

Understanding these waves is therefore crucial for modeling and predicting the behavior of fluid systems across various scales. Interestingly, the dispersion relations for gravity waves (1), inertial waves (2), and inertia-gravity waves (3) share similar properties. In particular, the phase and group velocities are orthogonal for plane waves and no characteristic length is prescribed. This mathematical analogy between rotating and stratified fluids has been well-known for more than 75 years. In his review, Veronis [22] describes this parallel and shows in different examples how results from one system can be analyzed and understood in terms of the behavior in the analogous system. More recently, the similarities among models for rotating fluids, stratified flows and even flows in magnetohydrodynamics have been used to understand in a unified manner the problem of weak turbulence of, respectively, inertial, gravity, and Alfvèn waves [23]. Differences, however, still exist and have to be taken into account. The major one is the motion of the fluid particles in a wave. Indeed, for a plane wave, the wave is made of rectilinear oscillations for internal gravity waves while it is made of anticyclonic circular oscillations for inertial waves, implying a 3D motion in the latter case, contrary to the former (see in Maurer [24, Fig. I.3]). Since the first experimental validation of the dispersion relation for internal gravity waves [25] and for inertial waves [26], they have been the object of many theoretical, numerical, and experimental studies in the last decades. In this review, we discuss recent experimental studies on either inertial waves or gravity waves in different setups using either non-rotating stratified fluids or rotating homogeneous (unstratified) fluids; a few cases of rotating-stratified configurations are also discussed. We focus on three main setups: wave beams, axisymmetric waves, and, finally, wave attractors. We will pay particular attention to studies involving Triadic Resonant Instability (TRI).

1.1. *Governing equations*

In this article, we consider a linearly stratified incompressible fluid subject to a global rotation at a rate $\Omega = f/2$ around the vertical axis, defined by the unit vector $\mathbf{e}_z$. We consider the case in which the background stratification is constant and parallel to the axis of rotation, i.e. the background density $\bar{\rho}$ is a linear function of z, characterized by the constant buoyancy frequency $N = \sqrt{-\frac{g}{\rho_0}\frac{\partial \bar{\rho}}{\partial z}}$ with ρ_0 the mean density. In the rotating frame of reference, the dynamics of such flow is described by the Navier–Stokes and mass conversation equation under the Boussinesq approximation

$$\rho_0\left(\frac{\partial \mathbf{v}}{\partial t} + (\mathbf{v}\cdot\nabla)\,\mathbf{v}\right) = -\rho_0 f\,\mathbf{e}_z\times\mathbf{v} - \nabla p' - \rho' g\,\mathbf{e}_z + \rho_0\nu\Delta\mathbf{v}, \tag{4}$$

$$\frac{\partial \rho'}{\partial t} - \frac{\rho_0}{g}N^2\mathbf{v}\cdot\mathbf{e}_z + \mathbf{v}\cdot\nabla\rho' = \kappa\Delta\rho', \tag{5}$$

$$\nabla\cdot\mathbf{v} = 0. \tag{6}$$

In these equations, $\mathbf{v}(\mathbf{x}, t)$ stands for the velocity field, ν the kinematic viscosity, κ the diffusivity of the stratifying agent. The pressure field p' is the pressure perturbation to the hydrostatic pressure incorporating the centrifugal acceleration. The density field ρ' is the difference between the total density field ρ and the density background stratification $\rho'(\mathbf{x}, t) = \rho(\mathbf{x}, t) - \bar{\rho}(z)$. As a result, the system forms a set of five equations with five unknown quantities: the velocity field $\mathbf{v}$, the

pressure perturbation p' and the density perturbation ρ'. In a given problem, ($\mathbf{v}$, ρ', p') are the solutions of equations (4)-(6) completed with boundary conditions.

Introducing U a characteristic velocity amplitude and L a characteristic length, the previous equations exhibit various dimensionless numbers, which are important to characterize the flows. In what follows, we will consider waves and therefore, the characteristic length will be related in most cases to the wave length, $2\pi/|\mathbf{k}|$, with $\mathbf{k}$ the wave vector. Due to the anisotropy of rotating and/or stratified flows, it is important to consider separately the components that are perpendicular and parallel to the direction of the stratification/axis of rotation. We denote $k_\perp = 2\pi/\lambda_\perp$ (respectively $k_z = 2\pi/\lambda_z$) the perpendicular component (respectively parallel component) to $\mathbf{e}_z$. For each dimensionless number described below, two can be defined using the horizontal or the vertical wavelength, the subscript $_j$ standing for $_\perp$ and $_z$. Note that, in most stratified turbulence theories, the anisotropic limit $\lambda_z \ll \lambda_\perp$ is considered [27]. This limit is indeed relevant for geophysical flow. On the contrary, in experiments, $\lambda_\perp \sim \lambda_z$.

- The Froude number, $\mathrm{Fr}_j = \frac{U}{\lambda_j N}$, represents the ratio between the buoyancy time scale and the inertial time scale. The regime where internal gravity wave propagation takes place is the small Froude number regime.
- The Rossby number, $\mathrm{Ro}_j = \frac{U}{2\Omega\lambda_j}$, compares the advection term to the Coriolis term. The regime where inertial wave propagation takes place is the small Rossby number regime.
- The ratio $N/2\Omega$ compares the importance of stratification with rotation.
- The Reynolds number, $\mathrm{Re}_j = \frac{U\lambda_j}{\nu}$, characterizes the separation between laminar and turbulent flow.
- The Schmidt number, $\mathrm{Sc} = \nu/\kappa$, compares the viscous effects with the diffusive ones. In the ocean, for salt water, $\mathrm{Sc} \approx 700$.
- The Ekman number is defined as $\mathrm{Ek} = \frac{\nu}{2\Omega L^2} = \frac{\mathrm{Ro}}{\mathrm{Re}_j}\frac{\lambda_j^2}{L^2}$ with L a characteristic global scale of the flow. It characterizes the importance of viscous forces compared with Coriolis forces. It is associated to phenomena emerging from boundary layers.
- The Richardson number, $\mathrm{Ri} = \frac{g}{\rho_0}\frac{|\partial_z\rho'|}{(\partial_z U)^2}$, compares the potential energy due to buoyancy with eddy kinetic energy. Small Richardson numbers are associated to overturning and mixing [28, 29].

An interesting regime is the one for which $\mathrm{Re} \gg 1$ while $\mathrm{Fr} \ll 1$, with low-frequency waves $\omega/N \ll 1$. This regime corresponds to stratified turbulence. For forcing frequencies ω/N comparable to the Froude number, the dynamics falls in the strongly stratified turbulence regime, relevant notably for the atmosphere. If ω/N is large compared to the Froude number, i.e. if $\mathrm{Fr} \ll \omega/N \ll 1$, the dynamics is dominated by weakly interacting non-linear internal gravity waves and corresponds to a weak wave turbulence regime. These regimes are the object of the review [30].

In the linear inviscid limit, this set of equations has wave solutions with the following dispersion relation

$$\omega^2 = N^2 \sin^2\beta + f^2\cos^2\beta = f^2\frac{k_z^2}{k^2} + N^2\frac{k_\perp^2}{k^2}, \tag{7}$$

The angle β is the angle between the vertical and the wave vector. This dispersion relation is illustrated in Figure 1 using (ω, β) polar plane. The angle β is associated to a single value ω while a value of ω is almost always associated to 4 values of the angle β corresponding to the 4 quadrants of the oft-cited Saint Andrews cross. In the special case $f = N$, only a single value $\omega = N = f$ is allowed and valid for all angles. This schematic illustrates the symmetry between N and f.

The dispersion relation (7) leads to different features. First of all, it limits the accessible values of the frequency ω to either $f < \omega < N$ or $N < \omega < f$. Outside these ranges, internal waves are evanescent. The low frequency domain can however be populated by other types of waves, such

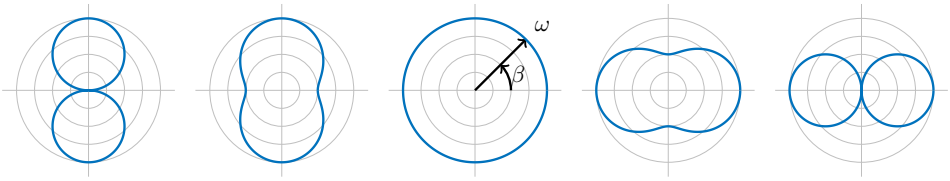

Figure 1. Dispersion relation (7) plotted in the (ω, β) polar plane, for dimensionless parameters N and f: to each angle β corresponds a unique frequency ω given by the blue curve (extracted from [31]).

as Rossby waves which exist in the presence of a zonal mean flow. Another feature of these types of waves, the phase velocity $\mathbf{c}_\varphi$, aligned with the wave vector, and the group velocity $\mathbf{c}_g$ are orthogonal. Importantly, as already mentionned in the introduction, the value of ω does not determine the wave length, which depends on many phenomena such as boundary effects or non-linear effects. This final remark implies that a particular attention must be paid to the choice of the wave maker to generate controlled gravity or inertial wave beams, as will be discussed in Section 1.2.

An important feature in the comparison between internal gravity and inertial waves is the wave structure itself. To explain this difference, let us first consider a plane wave characterized by a single wave vector $\mathbf{k}_0$. The fluid motion for internal gravity waves is rectilinear, perpendicular to $\mathbf{k}_0$, and contained in the $(\mathbf{k}_0, \mathbf{e}_z)$ plane. In contrast, due to the Coriolis term, the inertial wave field is characterized by anticyclonic oscillations in the plane perpendicular to $\mathbf{k}_0$ and is therefore inherently three dimensional. In the following, for both inertial and internal gravity waves, we will call 2D wave any superposition of plane waves for which all the wave vectors are localized in a single plane containing $\mathbf{e}_z$. The velocity field will therefore be uniform in the direction normal to this plane. Note that, with this definition, an inertial wave will be considered as a 2D wave even if the three components of the velocity field are non zero. Such differences could lead to different behaviors as we will describe in the rest of this article.

Dissipation effects take place through viscosity or salt/temperature diffusion. In almost all experiments, this influence of viscosity has a negligible effect on the relation between ω and the direction of the wave vector. However, as the waves propagate, viscosity results in energy dissipation and attenuation of the wave. This dissipation has a characteristic time scale $1/(\nu k^2)$ and is therefore large for short wave lengths. It explains why viscosity has to be taken into account in laboratory experiments compared to geophysical and astrophysical flows. A self-similar solution describing the propagation of a viscous wave beam was found independently for rotating fluids [32] and for density-stratified fluids [33]. Near boundaries, such as the ocean floor or a container wall, viscosity plays a significant role in modifying gravity/inertial wave behavior. The dissipation near topographies clearly matters in the global energy budget [34]. Both inertial waves and gravity waves can be affected by the presence of a viscous boundary layers, which in turn can be modified due to the presence of gravity/inertial waves, leading to intricate patterns of motion and transport within these fluid systems [35–39]. For internal gravity waves, a strong mean flow will modify the wave field and may in turn be generated due to non-linearities of internal gravity waves in 3D [20, 40] or due to streaming in the viscous boundary layer as predicted theoretically [41] and observed experimentally [38]. The equivalent feature for rotating flows is the existence of zonal flows, a characteristic phenomenom of forced rotating flows. They are generated by different mechanisms such as non-linearities in the Ekman

boundary layer [42] or non-linear inertial waves [43]. Such axisymmetric mean flows have been observed experimentally [44].

Finally, an important phenomenon that needs to be considered in stratified fluids is internal-wave driven mixing [45]. When the wave amplitude is large enough, the shear associated with it can be characterized by a small Richardson number ($Ri < 0.25$), inducing overturns that can lead to mixing. This can be particularly true if TRI is present, contributing to energy transfers to smaller scales, resulting in a more efficient mixing. This mixing can be seen as a problem in experiments since the linear stratification cannot be conserved contrary to numerical simulations. However, mixing is critical for climate models [46]. In numerical models, mixing and associated turbulence are usually linked to subgrid scale internal wave processes. It is therefore crucial to understand the mixing caused by internal waves and to properly parameterise the mixing efficiency. To that extent, various experiments have been performed at ENS de Lyon to study the influence of TRI on mixing [47, 48].

1.2. *Experimental techniques*

Internal gravity waves in the laboratory require a stratified medium, which is generally achieved using salt as the stratifying agent, easier to manipulate than temperature. The filling of the tank is performed via the so called two-bucket method [49, 50], which in its initial version produces a linearly stratified medium in a tank whose horizontal section is vertically uniform, but which can actually be generalized, using computer-controlled pumps, to create non-linear density profiles, or to produce a linear profile in a tank of vertically varying section [51]. Stewart et al. [52] have recently developed a derivation of this method, allowing to use temperature stratification.

As to rotating fluids, one "simply" needs to place a tank on top of a rotating table, which of course implies a number of technical challenges, including dealing with spin-up processes, non horizontal isobars, mechanically restraining the tank and all the measuring devices and allowing proper communication of power and data between the non-rotating and the rotating frame. The spin-up process, in particular, is rendered more complex when the fluid is also stratified [24], since the stratification prevents Ekman pumping motion, which is the major driving motion to attain solid body rotation during a spin-up.

Once the supporting medium is ready, a device is necessary to create the perturbation to this medium that will generate the wave. Almost 60 years ago, Mowbray and Rarity [2] were the first to produce internal waves in a laboratory experiment, using a sphere oscillating vertically in a linearly stratified fluid. Since then, experimentalists have been very creative in improving the design of the wave generators. Table 1 is an attempt to summarize and classify these various types of wave generators.

In laboratory experiments, internal waves can be observed thanks to the following techniques:

- Dye lines, showing the motion of iso-density lines (or isopycnals), mainly qualitative;
- Particle Image Velocimetry (PIV), based on following in time the motion of patterns of tracer particles, giving access to the velocity field;
- Synthetic Schlieren, based on the apparent displacement of a pattern placed behind the experimental tank, linked to the change in refraction index of the fluid, associated with the density perturbation accompanying the wave propagation. It gives access to the density gradient field [53] or to the whole density field [54] (only possible for gravity waves);
- Planar Laser Induced Fluorescence (PLIF), using a laser-excited fluorescent dye as tracer for density, allowing to measure directly the density field. It can be coupled to PIV, using the same laser plane, to get access to density-velocity correlations and therefore density fluxes, important for studies of mixing [47] (only possible for gravity waves).

Table 1. List of experimental gravity and/or inertial wave generators, organised by type of wave form generation.

	Category	Description	Type of wave	Example reference
I	Whole tank oscillation	Up and down motion	Global mode or self-similar wave beam	[55]
		Libration		[56]
II	Global boundary motion	Oscillating rigid wall	Guided wave	[37, 57]
		Oscillating rigid lid		[58]
III	Oscillating object	Oscillating cylinder	Self-similar wave beam	[25, 59]
		Oscillating sphere		[60]
		Oscillating torus		[61]
		Multiple oscillating objects		[62]
		Tidal motion on a fixed obstacle		
				[63]
IV	Towed object	Towed object	Wave beam	[64]
V	Oscillating plates	Linear device	Versatile wave form	[65]
		Independent oscillating plates		[66–68]
		Axisymmetric oscillating plates		
				[69]
VI	Local boundary deformation	Deformable tank	Specific purpose	[70, 71]
VII	Liquid interface motion	Turbulent underlayer	Uncontrolled	[72]
		Convective underlayer		[73]

The two most common techniques, PIV and Schlieren, allow quite easily for an extraction of wave frequency content and spatial structure, using respectively Fourier transform (or time frequency analysis [74] when time-dependence is relevant) and Hilbert transform [75]. Many experiments require to estimate or to measure quantitatively the amplitude of the primary wave. One cannot rely on the amplitude of the wave generator motion, since there is an efficiency factor that comes into play and that depends strongly on frequency, wave form and experimental conditions. For the Schlieren technique, such measurement requires integration of the mass conservation equation, which in general cases with multiple waves is not a simple task. In the same way, for PIV measurements, a direct estimate of the kinetic energy of the whole velocity field can easily be computed. However, quantifying the amplitude of a specific wave among other waves in interaction can be difficult.

Among the various methods used to extract a wave amplitude, Mathur et al. [76] studied transmission and reflection of internal wave beams across a transmission region and took a Fourier transform of the reflected and transmitted wave fields along appropriately chosen transects. Maurer [24] measured wave amplitudes by looking at the maximum of the velocity over a given spatial area, and Supekar et al. [77] utilized the distribution of maxima of amplitudes for a velocity field in a widespread two-dimensional beam. Boury et al. [78] first performed a fit of the wave form to the expected spatial profile as a function of time, thus extracting a wave amplitude as a function of time, before averaging in time the obtained amplitude, choosing a time window where the process was as stationary as possible. When the amplitude of two different waves of same frequency must be estimated (in the case of wave reflection for example), a method based

on the signal processing technique called Variable Mode Decomposition has been adapted successfully [79]. In the case where time stationarity is not achieved in the observed experiment, Boury et al. [80] developed a method based on using Hilbert transform times series and root-mean-square averaging to obtain a time dependent amplitude of the waves. Finally, in the case where synthetic Schlieren is used to observe the waves, Grayson et al. [81], based on previous developments [64, 82], used integrated components of the density gradient field, to which they apply a root-mean-square and spatial average.

2. Internal Wave Beams in a Square Geometry and its Instability

During the years 2010-2015, a series of studies [40, 83, 84] was undertaken by a group at ENS de Lyon, jointly with a group at Université d'Orsay (now Université Paris-Saclay), where the generation of plane beams of internal gravity waves (in Lyon) and inertial waves (in Orsay) was obtained using the same wave generator (linear oscillating plates, type V of Table 1), allowing for interesting comparisons between both types of generated waves, and in particular regarding the Triadic Resonant Instability of the corresponding wave beams.

2.1. *Generation of Gravity Versus Inertial Waves*

In both cases, the generation of the waves was very similar, using the wave generator described in [65], placed in a tank, either non-rotating but linearly salt stratified (in Lyon) or non stratified but lying on top of a platform rotating at rotation rate Ω (in Orsay). It was actually the same device, which travelled from Lyon to Orsay. In both cases, the generator configuration was set to excite a plane wave beam, with 3 to 4 wave lengths of about 7 cm each along the whole height of the generator, with a tapering amplitude at each end to avoid spurious emission of internal waves.

However, a main difference lies in the generation process, since the fluid motion in the case of internal gravity waves is a simple oscillating translation in the direction of the group velocity, whereas fluid particles describe anticyclonic circular translation in the case of inertial waves. As a consequence, for inertial waves, the oscillating plates of the wave maker only force the longitudinal component of their circular motion, while the lateral component is let to freely adjust according to the spatial structure of the wave solution. This makes the generator less efficient in producing inertial waves, compared to gravity waves. A detailed description of the added difficulty when producing inertial waves with this generator, with an efficiency depending strongly on generator amplitude and wave length can be found in the appendix of [85, Chapter 3].

In order to make up for that difficulty, the generator angle was adapted to the oscillating frequency ω, so that the plate motion would actually be in the exact direction of the longitudinal component of the wave motion. Note that this solution is not applicable to the case of gravity waves, since reclining the generator, with a change of inclination for each frequency studied, would be complicated and would also rapidly destroy the stratification.

In the case of inertial waves, it turned out that in order to vary the wave angle, set by the ratio $\omega/f = \omega/2\Omega$, it was easier to change the global rotation of the table, rather than changing the generator frequency. For gravity waves, of course, changing the stratification was not an option and it is the wave frequency ω that was varied.

One last point of comparison: in both cases, the generator was parallelepippedic. While for gravity waves, which have a perfect 2D behaviour, this is not a problem, it becomes more tricky with inertial waves, which have inherent 3D motion and the tank shape is not really adapted, with lateral walls restraining the transverse motion. For this reason, while the tank used for gravity

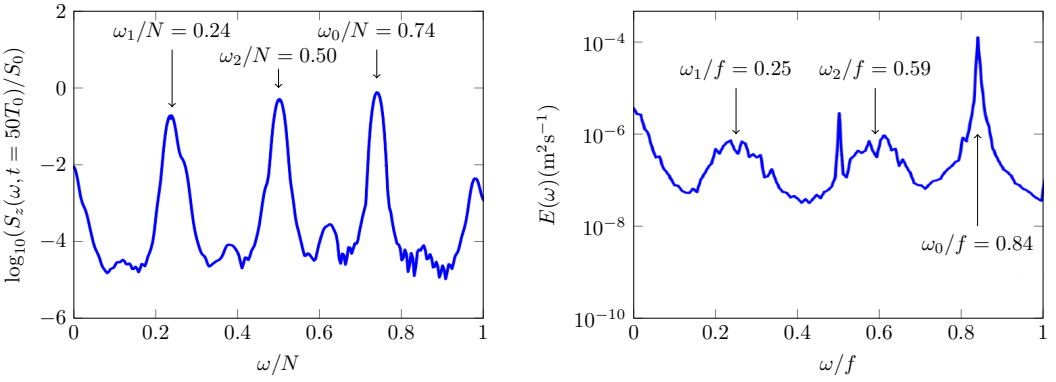

Figure 2. Examples of frequency spectra showing TRI. (Left) Frequency spectrum for internal gravity waves ($N \neq 0, f = 0$), from [83]. (Right) Frequency spectrum for inertial waves ($N = 0, f \neq 0$), from [40]. In the latter case, a narrow peak corresponding to the rotation frequency of the table (thus at $\omega/f = 0.5$) is visible, linked to mechanical noise of the table.

waves was narrow (2 wave lengths), in the case of inertial waves, the tank was much wider, with a width of about 10 wave lengths.

As we will show later, in spite of these differences, the production of the waves and the characteristics of the instability via resonant interaction are very similar.

2.2. *Instability of the Wave Beams*

Already in 1967, Davis and Acrivos [86] showed experimentally and theoretically that, due to the non-linear terms of the wave equations, internal waves are unstable to infinitesimal perturbations, which grow to form temporally and spatially resonant triads between the primary wave (indicated in what follows by index 0), and two secondary waves (indicated by indices 1 and 2). These resonant conditions write respectively

$$\omega_0 = \omega_1 + \omega_2, \tag{8}$$

$$\mathbf{k_0} = \mathbf{k_1} + \mathbf{k_2}. \tag{9}$$

This instability is now referred to as *Triadic Resonant Instability* (TRI). The analytical derivation for the plane wave solutions of the non-linear wave equations can be found in Dauxois et al. [20]. For a given primary wave vector of components (ℓ_0, m_0), combining the dispersion relation of the waves with the temporal resonance condition (and eliminating one of the two secondary wave vectors using the spatial resonance condition), one obtains the following equation for the components (ℓ_1, m_1) of the remaining secondary wave vector

$$\frac{|\ell_0|}{\sqrt{\ell_0^2 + m_0^2}} = \frac{|\ell_1|}{\sqrt{\ell_1^2 + m_1^2}} + \frac{|\ell_0 - \ell_1|}{\sqrt{(\ell_0 - \ell_1)^2 + (m_0 - m_1)^2}}. \tag{10}$$

The set of solutions of this equation can be represented by a resonance locus ([20, Figure 2.a]) defined as the possible locations in wave vector space of the tip of vector $\mathbf{k}_1$. We recall the typical shape of this locus, with examples of the vector triads $\mathbf{k}_0$, $\mathbf{k}_1$, and $\mathbf{k}_2$ in the insets of Figure 3 (left).

The TRI instability was observed in several laboratory experiments [87–89] with increasing details thanks to progresses in fluid motion imaging, using in particular PIV and synthetic Schlieren in the last decade. This instability was shown to play a role in oceanic energy transport and vertical mixing [90, 91].

Here again, the joined study performed by the Lyon and Orsay groups using the same wave generator provides an interesting view on the TRI instability in the respective case of internal gravity waves and inertial waves. In both cases, with a large enough amplitude – typical wave velocity of the order of 2 to 3 mm.s^{-1}, or in other words dimensionless quantity ψ_0/ν (equivalent to a typical Reynolds number of the flow), of the order of a few tens, where ψ_0 is the stream function amplitude of the wave – the instability starts after 20 to 40 generator periods.

Figure 2 shows the frequency spectra of the wave system after the onset of instability, on the left for the gravity waves and on the right for the inertial waves. Three main peaks are observed, corresponding to the primary and two secondary waves. In both cases, the temporal resonance condition is verified. However, the secondary peaks are much broader for the inertial wave case than for gravity waves. A possible explanation for this observation is given in Section 4.4.

One of the interesting features of TRI, in the oceanic mixing context, is that it allows for a transfer of energy to smaller scales, without the necessity of a turbulent energy cascade. That happens in particular when both secondary waves have larger wave vectors, compared to the primary wave: $\kappa_{1,2} > \kappa_0$, where κ is the modulus of the wave vector. This is the case, in general, when the solutions belong to the external branches of the resonance locus (see example in top inset of Figure 3 (left)). In contrast, when the solutions are on the central part of the locus, the transfer goes both directions, with $\kappa_1 > \kappa_0 > \kappa_2$, or vice-versa (see example in bottom inset of Figure 3 (left)).

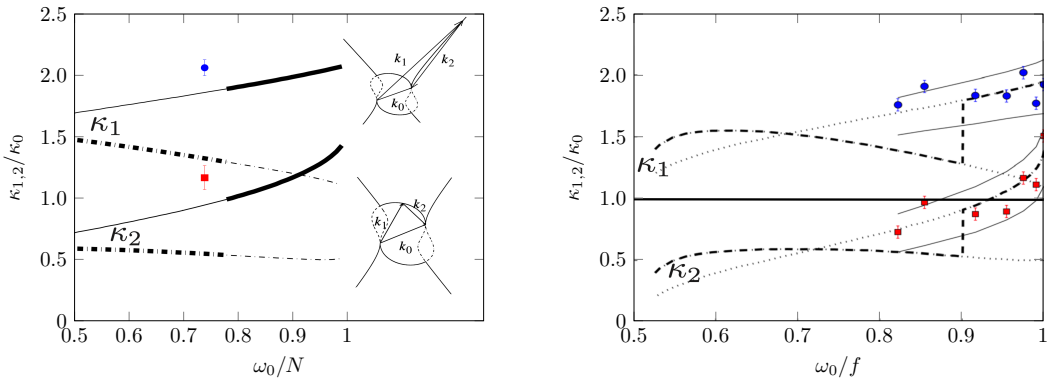

Figure 3. Normalized wave numbers $\kappa_{1,2}/\kappa_0$ of the secondary waves, as a function of the primary wave frequency ω_0. (Left) Gravity waves, adapted from[83]. (Right) Inertial waves [40]. The lines represent theoretical predictions, computed for the wave dimensionless amplitude $\psi_0/\nu = 28$ (left) and $\psi_0/\nu = 37$ (right). The insets on the left plot show two typical examples of the resonance locus. As illustrated in this inset, the solid lines on the left plot (upward going dotted lines on right plot) represent the case where the secondary wave vectors are on the external branches of the resonance locus, while the dashed lines on the left plot (mostly downward going dotted lines on the right plot) represent the case where the secondary wave vectors are on the central part of the locus. Between these two types of solutions, the one that has the largest growth rate is represented by a thicker line. Filled circles and squares with error bars correspond to experimental measurements. The two solid thin lines on the right plot show the allowed range around the dotted curves, determined by considering an uncertainty of ±50% on the wave amplitude.

Both studies mentioned earlier delved into this issue. For a given wave amplitude and for each normalised frequency ω/N of the primary wave, the relative magnitudes $\kappa_{1,2}/\kappa_0$ of the secondary wave vectors that correspond to the largest growth rate of the instability were computed, both in

the case of the external and central branches of the resonance locus. The result is presented in Figure 3, on the left plot for internal gravity waves [83] and on the right plot for inertial waves [40]. In addition, a thickening of the lines highlights the case (between central and external branches) with highest growth rate. There is a transition from the central to the external branch, at a frequency around $\omega/N = 0.77$ for gravity waves and $\omega/f = 0.79$ for inertial waves. Experimental points are also shown, with colored symbols. Interestingly, in both cases, even below the transition frequencies mentioned above, the experimental solutions seem to stay on the external branch, with, mostly, an energy transfer towards smaller scales, except at the lowest frequencies where TRI was observed in the case of inertial waves. Note that for gravity waves, were only one experimental point is shown, the magnitude of the wave vectors is slightly larger than predicted.

In a laboratory experiment of typical sub-meter size, the viscosity of water is such that small scale waves are damped quickly and secondary waves with wave vector magnitude above a few times the primary wave vector magnitude are never the most unstable solution (see [20, Figure 2.c]) and are therefore never observed. However, the opposite trend can be observed in Figure 3, where wave vectors longer than expected were measured and the solution on the central branch of the resonance locus, where wave vectors are shorter, was never observed.

This could be explained by a finite-size effect. This effect was described in Bourget et al. [84] and relates to the fact that in finite-size beams with a width equal to only a few wave lengths, the secondary waves, which have a group velocity with a different direction than the primary wave, leave the interaction region, located within the primary wave beam width, before the instability has time to grow. This effect is of course enhanced when the waves have a large group velocity, which is the case of waves of small wave vectors, since group velocity increases when wave vector amplitude decreases. For this reason, one can understand that the solutions on the central branches of the resonance locus, which, for infinitely wide beams, have a larger growth rate below the transition frequency, are not observed in the experiments, since the actual growth rate, taking into account the finite size effect, is reduced (see equation 3.7 in [84]).

2.3. *Variability of the Triadic Resonant Instability*

A recent study by Grayson et al. [81] focused on the long-term fate of TRI in the case of narrow beams of internal gravity waves. The authors used a large scale tank (11 m wide) to prevent interactions between the beam and its reflections and they took advantage of the very versatile "magic carpet" wave generator built in Cambridge (type V of Table 1, [66]). By doing a refined analysis of the characteristics of the secondary waves of the TRI, they showed that there exists an important variability in amplitude, frequency and wave vector of these secondary waves. This variability takes place both in time and space.

This is illustrated in Figure 4, showing the power spectral density at the function of time and frequency (left plot) and as a function of the secondary wave vector horizontal components and of the height in the tank (right plots). On the left plot, one can observe that while the primary wave frequency maintains a constant value at the forcing frequency Ω_0/N=0.62, both secondary frequencies fluctuate in time, while conserving the resonance property $\omega_1 + \omega_2 = \omega_0$. Note that frequencies around 0.0, 0.8, and 1.0 come from higher order interactions. In order to better understand the underlying modal structure of the observed beams, Grayson et al. decomposed the flow field using Dynamic Mode Decomposition (DMD, white line superimposed in the time-frequency plot), confirming the observed variability. A similar variation in frequency has been witnessed by both Bourget et al. [83] and Brouzet et al. [92] in their experimental studies. One can also observe at certain times (in particular between 100 and 200 T_0, as well as between 200 and 300 T_0), other pairs of secondary beams appearing and then merging with the continuous mode,

in the form of convergent "wisps" on the ω_1/N and ω_2/N bands. The authors have checked that in such cases, the triadic resonance in frequency persists across all the spectrum.

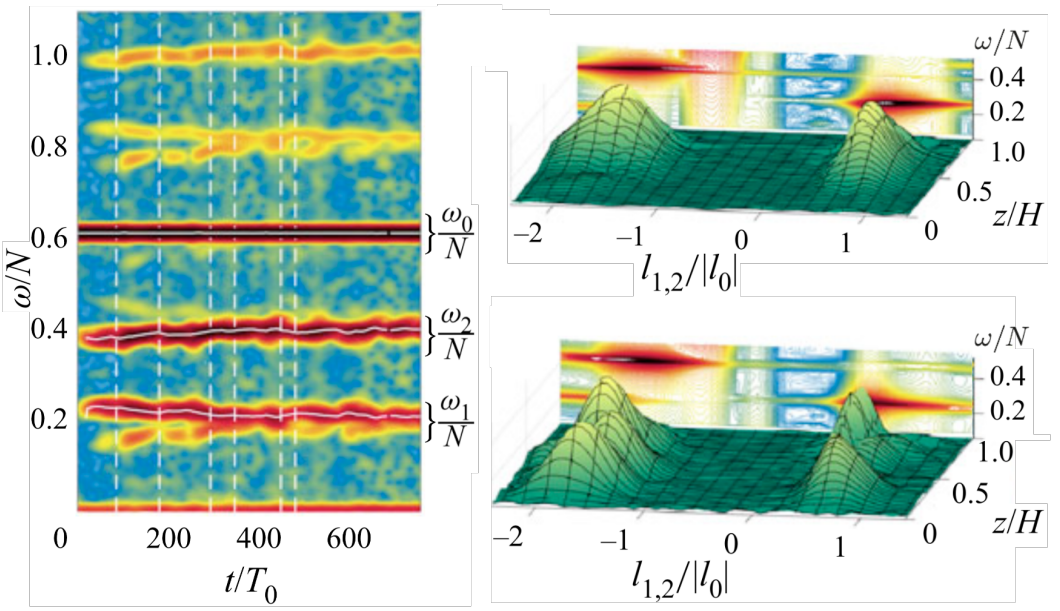

Figure 4. (Left) Time-frequency spectra (log scale of normalised spectral density) for a long term experiment. The dominant frequencies obtained from the DMD frequency decomposition are overlaid in white. (Right) For the same experiment, distribution of energy in the ℓ/ℓ_0 space and over the non-dimensional height in the domain z/H. (top) $t/T_0 = 83$, (bottom) $t/T_0 = 481$. Both the surface plot colour and the height of the peaks show the power spectral density. The left (right) "bump" corresponds to ℓ_2 (ℓ_1). The background plot shows the power spectral density at the same instant in time in the Fourier plane of horizontal wave number component and frequency. Adapted from [81].

The right plot shows, at two different times, the distribution of energy along the horizontal component of the wave vector and across the height of the tank. One can observe that at the earlier time (top figure), the TRI is mostly localised in the upper part of the tank, with the ℓ_2 component at a value around $-2\ell_0$ and the ℓ_1 component at a value around $0.8\ell_0$. Note that the two secondary waves can be identified on this plot thanks to the background plot, showing the distribution of energy in the (ℓ,ω) plane, the wave with largest frequency being identified with index 2 ($\omega_2 > \omega_1$, see left plot). At a much later time (bottom figure), towards the end of the experiment (which lasted $682T_0$), one can see that the distribution of energy over ℓ and z have evolved, with in particular different values of ℓ_1 and ℓ_2 depending on z/H, as well as a central region (around $z/H = 0.5$), where no secondary waves are present.

Grayson et al. [81] interpret these observations by a finite-size effect, using a model quite similar to the one presented in Bourget et al. [84], taking into account how the secondary waves exit their interaction region with the primary wave due to their group velocity. However, the main difference with the model of Bourget et al. [84] is that the instability is allowed to be a function of space, and not only time as was the case in the previous model. The authors show that including this feature in the model actually results in the observed variability. In addition, they show that with the parameters of the experimental study, the ratio between the residence time of the secondary waves in the interaction region and the development time of the instability is close

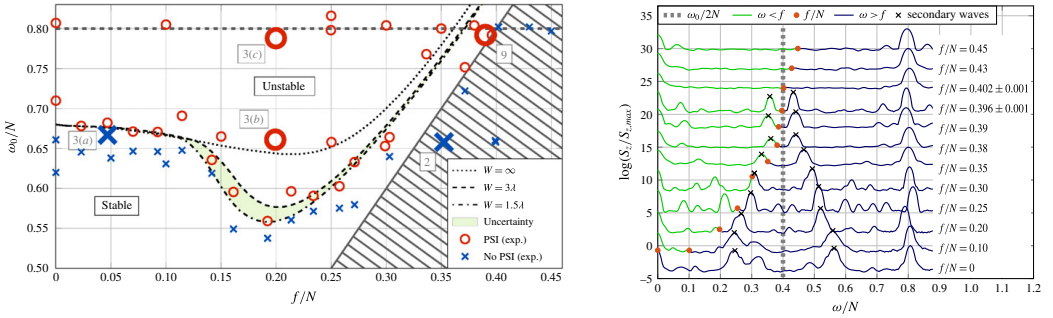

Figure 5. (Left) Experimental observations showing the triadic resonance stability or instability of a primary wave of dimensionless frequency ω_0/N at Coriolis parameter f/N. The instability threshold in this $(f/N, \omega_0/N)$ phase space is shown by various curves, depending on the beam width. The hatched zone corresponds to a forbidden zone for TRI (see text). (Right) Renormalized amplitude of the Fast Fourier Transform of the vertical gradient of density for various values of f/N. For the sake of clarity, the spectra were shifted vertically. The vertical dashed line indicates $\omega/N = 0.4 \simeq \frac{1}{2}\omega_0/N$. On each spectrum the peak on the right represents the primary wave, daughter waves correspond to the other peaks. Extracted from [93].

to one, so that the TRI is actually very sensitive to the actual properties of the secondary beams. As a result, preferential selection of triads is locally determined. As one triadic interaction decays, another forms, but this time at a different physical location and with new secondary beam properties. This explains why, experimentally, modulations are observed not only in physical space but also in Fourier space.

2.4. *What Happens with TRI when Combining Stratification and Rotation ?*

An extensive comparison of the characteristics of TRI between gravity and inertial waves has been presented in Section 2.2, mainly based on the joined studies of the Lyon and Orsay groups. A question remains: how is, for example, the TRI for gravity waves modified when rotation is added? This study has been performed in [93], where the same experiment used in [83, 84] was placed on a rotating table, which was rotated at values of f/N between 0 and 0.45.

The main results are summarised in Figure 5. The left plot represents the phase space (f/N, ω_0/N), where the instability threshold, computed including the effect of rotation in the finite-width analysis of Bourget et al. [84], is represented by several lines, depending on the beam width (infinite, 3 wave lengths and 1.5 wave length). One can observe that - as expected since the group velocity, at the heart of the finite-width effect, decreases with the rotation rate - the instability threshold lowers when rotation increases, all the more when beams are narrow. This effect only takes place on a limited range of rotation rates, since in this phase space there is an exclusion region for TRI (hatched). This is due to the fact that, as rotation rate increases above $\omega_0/2$, with secondary wave frequencies that have to be larger than f, it implies $\omega_0 > 2f$, which is not possible for propagating waves. As a result, there is a value of f/N for which the threshold is minimum, reminiscent of the critical latitude phenomenon described in MacKinnon et al. [90]. Experimental data points are shown, with symbols indicating if TRI was observed or not, and they are in very good agreement with the analytical predictions given by the smooth curves.

On the right plot of Figure 5, the frequency spectra for all values of rotation rates are shown, allowing to observe the evolution of the secondary frequencies with f/N. As rotation increases,

the frequencies of the two secondary waves get closer (and therefore closer to $\omega_0/2$). As the rotation rate gets very close to the limit of the forbidden region ($\omega_0/2$), the secondary wave of lowest frequency surprisingly falls below f. An explanation of this result could be the existence of a non-zero out-of-plane component of the wave vector. This has been discussed in Mora et al. [94], who show that when rotation is present, the maximum growth rate is obtained with a non-zero component of the wave vectors in a direction perpendicular to the primary wave beam. This result is attributed to the 3D structure of inertial waves. Indeed, while theoretical analysis have shown that coplanar triads always display the highest growth rates for TRI of internal gravity waves [95], in contrast, for inertial waves the possibility of an out-of-plane component of the secondary wave vectors is still an open question both theoretically and experimentally.

3. Axisymmetric Waves

Beyond two-dimensional (2D) wave beams, various recent studies have delved into three-dimensional (3D) internal waves assuming that they would exhibit peculiar dynamics. The drive to study such wave fields is, interestingly, both experimental and theoretical to investigate whether purely 3D effects may exist, either in the linear or in the non-linear regime. Besides in-situ measurements of axisymmetric wave fields [96, 97], it is interesting to note that various laboratory systems generate such wave fields, e.g. vertically oscillating spheres [98, 99] or impacting plumes [100].

In what follows, we will use the distinction made in [101] between axisymmetric waves that are invariant by rotation (θ-independent, where θ is the orthoradial angle in the horizontal plane) and cylindrical waves that allow for an orthoradial dependence (θ-dependent). Axisymmetric waves are a particular class of cylindrical waves, easier to generate and study experimentally.

Axisymmetric wave fields have traditionally been experimentally excited using a vertically oscillating sphere and exploring the shape of the wave beams [2, 98, 99, 102–104]. The radially decreasing amplitude and the viscous decay of the conical wave beam emitted by an oscillating sphere has been explored in laboratory experiments by Flynn et al. [99] showing good agreement with theoretical predictions. More sophisticated axisymmetric experimental geometries have later been investigated using a vertically [61] and a horizontally [105] oscillating torus, in which case a highly non-linear process occurs due to the three-dimensional geometric focusing, able to transport momentum and break into turbulence. None of these experimental configurations, however, readily permitted a change in the form nor the wave number of the wave field being excited. Versatile configurations have been obtained thanks to a cam-based axisymmetric wave [69] generator, derived from the planar wave generator developed by Gostiaux et al. [65] (see Table 1).

The experimental study of axisymmetric waves presents several difficulties. First, the fundamentally 3D geometry of the waves means that a complete characterisation requires visualizations both in the vertical and in the horizontal planes. A way to obtain this imaging is to elevate the tank and use an mirror inclined at 45 degrees below it (e.g. [69]). Second, to match boundary conditions with the axisymmetry of the wave field, it is more appropriate to use a cylindrical tank with the same geometry; to prevent optical distorsions, this cylindrical tank should then be enclosed in a larger tank of square cross section.

3.1. *Linear Dynamics*

Axisymmetric waves can be described in natural cylindrical coordinates (r,θ,z) by decomposing the velocity field into two horizontal (radial and orthoradial) and one vertical velocity compo-

nents, (v_r, v_θ, v_z). For practical reasons, it is instructive to introduce the stream function under a symmetric formalism

$$v_r = -\frac{1}{r}\frac{\partial(r\psi)}{\partial z} \qquad \text{and} \qquad v_z = \frac{1}{r}\frac{\partial(r\psi)}{\partial r}. \tag{11}$$

Neglecting non-linear and dissipative terms, the axisymmetric stream function satisfies a collapsed equation

$$\frac{\partial^2 \Delta\psi}{\partial t^2} + f^2\frac{\partial^2\psi}{\partial z^2} + \frac{N^2}{r}\frac{\partial^2(r\psi)}{\partial r^2} = 0, \tag{12}$$

whose solutions can be found analytically under the form of either a product of a radial Bessel function and a vertical exponential, or a product of a radial Hankel function and a vertical exponential. These are the counterparts of sine-cosine and exponentials for Cartesian modes and plane waves, respectively. Bessel-shaped wave fields describe modes; Hankel-shaped ones are more appropriate to describe converging or diverging conical wave fields.

The dispersion relation can be obtained thanks to a Hankel–Fourier transform on equation (12), yielding

$$\omega^2(\ell^2 + m^2) = f^2 m^2 + N^2\ell^2, \tag{13}$$

with ω the wave frequency, and ℓ and m the radial and vertical wave numbers.

Cylindrical wave fields satisfy a system of equations similar to equation (12), but with non-zero θ-derivatives. Solutions to these equations are called Kelvin modes [101, 106, 107]. They involve rotating and counter-rotating waves, and preserve the 2π orthoradial periodicity through a dimensionless, integer, orthoradial wave number p. The axisymmetric dynamics is recovered by setting $p = 0$. Interestingly, p does not appear in the dispersion relation (13) which thus remains the same for both axisymmetric and cylindrical waves. A thorough description of these Kelvin modes can be found in [101].

Horizontal axisymmetric modal wave fields, propagating vertically, are the easiest to study and characterize experimentally as the radial structure can be described under the simple analytical form of a single Bessel function. Similarly to Cartesian studies, axisymmetric modes can be obtained experimentally by enforcing appropriate boundary conditions with a tank of the same radial size as the wave generator. Such modes have been described in [78].

3.2. *Non-Linear Dynamics*

While the linear dynamics of axisymmetric waves remains fairly similar to the linear dynamics of Cartesian plane waves, strong differences have been evidenced in the non-linear regime both in stratified and in rotating experiments [24, 56, 101, 108, 109]. The analytical justification is two-fold: first, contrary to the plane wave case, the cylindrical Jacobians giving the non-linear terms are no longer anti-symmetric, due to the r-derivatives, preventing some terms to mutually cancel out; second, while the product of two exponentials (plane waves) or sine-cosines (Cartesian modes) can be expressed under the form of another exponential or sine-cosine, the product of two Bessel functions does not usually have a similar simple expression but rather yields a sum of Bessel functions. This is further complexified for waves with a non-zero orthoradial velocity v_θ (notably inertial waves), as the horizontal Laplacian introduces additional non-linear terms coupling the horizontal velocities $(v_r,\ v_\theta)$ [101]. These different terms bring several questions regarding the non-linear dynamics of axisymmetric and cylindrical waves, whether it be the subsistance of the triadic resonant instability in a similar formalism as with plane waves, or the possibility for other non-linear behaviors to arise due to the modification of the Jacobian structure.

3.2.1. *Triadic Resonant Instability*

Axisymmetric Triadic Resonant Instability (TRI) has been proposed as a natural extension of TRI, extensively studied in 2D for plane waves. Various experimental studies in axisymmetric geometry led to the observation of localized TRI whose resonant conditions, both temporal and spatial, are the same as for plane waves [101, 109]. This is due to the assimilation, locally, of the axisymmetric wave field with a Cartesian wave field when disregarding the overall geometry of the system imposed by the forcing or by the boundary conditions. As such, it does not provide clear indications on a totally cylindrical, fully developed, TRI that would preserve the imposed geometry of the system. In axisymmetric focusing experiments performed with an oscillating torus in a stratified fluid, [109] have shown that a primary wave field can lead to resonant subhmarmonics in agreement with the 2D TRI theory. However, other experiments led by Maurer et al. [24] in a stratified and rotating fluid suggested that the axisymmetry could be broken for the subharmonics and that they may not fully satisfy the spatial resonance conditions.

An analytical derivation of the resonance conditions involving three cylindrical wave fields (Kelvin modes) performed by [101] showed that a fully 3D TRI could exist, preserving the cylindrical geometry of the system, although with some modifications compared to the Cartesian case. First, the three waves have resonant frequencies ω and two exact spatial resonances, along the vertical (m) and orthoradial (p) directions. The p resonance along θ is particular insofar as the wave fields also have to satisfy a 2π periodicity, which necessarily leads to a discretized resonance. Second, the situation gets more complex along the radial direction, as exact resonances have been shown to exist only for sufficiently large wave fields whereas in configurations of small extent or in confined geometries quasi-resonances are more likely to appear. Lastly, due to an asymptotic divergence at the center of the domain, it is unclear whether waves are locally spatially resonant at $r = 0$.

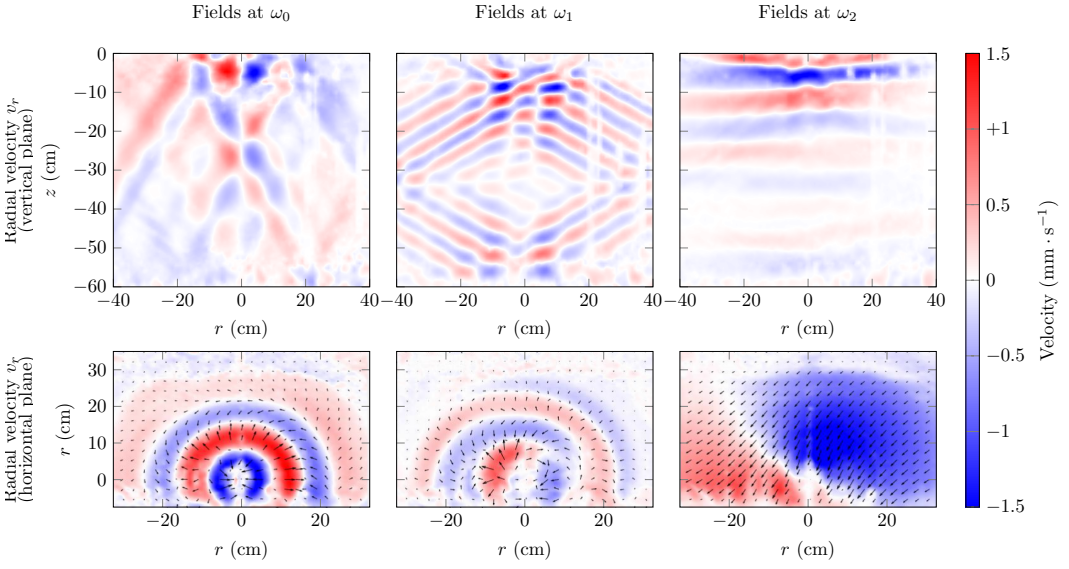

Figure 6. Experimental visualization of TRI for cylindrical wave fields. The top row shows the radial velocity field v_r in the vertical plane; the bottom row shows the same radial velocity field in the horizontal plane. From left to right: forcing wave field, at $\omega_0 = 0.80\ \mathrm{rad\cdot s^{-1}}$; first and second subharmonics at $\omega_1 = 0.50\ \mathrm{rad\cdot s^{-1}}$ and $\omega_2 = 0.30\ \mathrm{rad\cdot s^{-1}}$. Experiments conducted at $f = 0.29\ \mathrm{rad\cdot s^{-1}}$ and $N = 0.97\ \mathrm{rad\cdot s^{-1}}$ (adapted from [101]).

These results have been confirmed experimentally both in confined and in unconfined geometries [101]. Figure 6 shows an example of TRI obtained in an unconfined stratified-rotating experiment ($f = 0.29\,\mathrm{rad}\cdot\mathrm{s}^{-1}$ and $N = 0.97\,\mathrm{rad}\cdot\mathrm{s}^{-1}$), in which the forcing wave (shown in the first column) generates two resonant subharmonics (second and third columns). The velocity field in the horizontal plane shows that the two subharmonics are not axisymmetric. In addition, their time behavior shows that they have opposite orthoradial wave numbers. Interestingly, the axisymmetric forcing seems to lead to axisymmetric subharmonics if the fluid is stratified only; however, if the fluid is also rotating (as in the example shown in Figure 6), cylindrical subharmonics with a non-zero orthoradial wave number have been observed with the emergence of two contra-rotating subharmonic waves. Similar experiments performed in a confined domain have shown that TRI is slightly modified, as the radial wave numbers of the waves forming the triad can be quasi-resonant and not exactly resonant[101]. This result is consistent with the fact that boundary conditions are known to have a significant impact on the characteristics of TRI, as discussed in the case, for instance, of surface waves [110].

3.2.2. *Super-Harmonic Generation*

While for a single monochromatic plane wave, the self-interaction term $(\mathbf{u}\cdot\nabla)\mathbf{u}$ vanishes, this is no longer the case for axisymmetric wave fields. A direct consequence is that axisymmetric waves can self-interact and transfer energy to waves at higher frequencies, contrary to Cartesian plane waves (self-interaction is only possible for plane waves if the stratification is non-linear [111]). This process generates super-harmonics, i.e. waves at frequencies 2ω, 3ω, ... from an axisymmetric wave field initially forced at ω. These super-harmonics are propagating if the primary forcing occurs at sufficiently small frequency so that the harmonic frequencies remain smaller than the cut-off frequency imposed either by f or N. Evidenced for the first time in the experimental study of [108], these harmonics remain axisymmetric if the fluid is stratified and non-rotating. The energy is then distributed onto several waves (cavity modes in the aforementioned study), that satisfy temporal resonance conditions but not necessarily spatial ones. As for TRI, this could be due to the enforcement of boundary conditions that prevail over the resonances.

4. Internal Gravity Wave/Inertial Wave Attractor

4.1. 2*D and* 3*D Reflection*

As underlined in the introduction, internal waves propagate along a double cone with a half top angle equal to β which is given by the dispersion relation (7). Such a property leads to a peculiar reflection law of these waves on a slope. Snell's reflection law, applicable e.g. for light waves and surface waves, prescribes that the reflected and the incident waves have the same angle with respect to the normal to the slope. This is not the case for internal waves (either gravity or inertial waves). The first conservation law in this case is given by the non penetrability condition, written as

$$(\mathbf{v}_r + \mathbf{v}_i)\cdot\mathbf{n} = 0. \tag{14}$$

This leads to the conservation of frequency and of the projection of the wave vector along the direction of the slope. As a consequence, the reflected and incident waves propagate along the same double cone.

In 2D geometry, this means that the reflected wave propagates in a different quadrant of the Saint Andrews cross. In addition, the reflection on a slope inclined with an angle α with the horizontal leads to focusing or defocusing, depending on the relative values of α and β and on

the direction of propagation of the incident wave. When focusing occurs, the wave length of the wave beam decreases by a factor

$$\gamma = \left| \frac{\sin(\alpha + \beta)}{\sin(\alpha - \beta)} \right| . \tag{15}$$

Assuming conservation of energy, the energy flux density is increased by a factor γ^2 and the reflected wave is therefore more prone to instability. Note that the case $\beta = \alpha$ is a singularity ($\gamma \to \infty$), the so-called critical reflection. It has been the focus of theoretical analysis [112] and experiments [79].

In three dimensions, the orthoradial angle is not imposed by the dispersion relation and is therefore not conserved. The derivation of the reflection law in this case has been performed for internal gravity and inertial waves following slightly different approaches [113–117]. The different derivations use three ingredients: non penetrability; propagation of the incident and reflected waves on the same cone and conservation of the horizontal component of the velocity normal to the slope. They have shown that the rays of waves change direction upon reflection and have the tendency to converge toward the upslope gradient.

4.2. *Wave Attractor*

In a closed domain with a particular geometry and for a specific range of frequencies, successive reflections of wave rays in the domain have been shown to converge on the same limit cycle, which is a geometric pattern, called wave attractor [118]. Theoretical predictions can be made using ray-tracing methods, in which the wave beam is assumed to be localized enough so that its propagation along the group velocity can be described by a geometrical ray path. The phenomenon of concentration of the energy on attractors in 2D geometries has been the subject of different mathematical studies [35, 119–121]. In the past years, different geometries leading to the possible existence of wave attractors have been investigated. These works have been summarized in a recent review [122].

In astrophysics, the link between wave attractors and trapped wave in the equatorial regions of rotating planets has been first considered [123–125]. Rotating spherical shells have been shown to be a generic geometry for inertial wave attractors [126, 127], which appear in numerical simulations [16]. The role of different features such as the behavior of the waves in the vicinity of the axis of rotation, the critical latitude phenomenon, and non-linearities have then been analyzed [128–131].

Even if different works have considered the possible existence of internal wave attractors in real stratifications and topographies using different geometries [82, 132–134], no field observations of attractors has been reported so far.

In the following, we will focus on the main experimental results obtained in 2D trapezoidal geometries and in an axisymmetric frustrum to show the difference and similarities between gravity and inertial wave attractors.

4.3. *Experiments in Quasi-2D Trapezoidal Domains*

Following his seminal theoretical study [118], Maas has collaborated in different experimental studies to visualize internal gravity wave and inertial wave attractors. There were first observed in a density stratified fluid using an oscillating tank [135]. Even though the structure of an inertial wave is three-dimensional, a linear attractor was also observed in the case of inertial waves, using as well an oscillating tank as generator [35, 115, 136]. Without dissipation, the energy density along the attractor tends to infinity due to multiple focusings. In a more realistic scenario, the energy is dissipated through viscous dissipation or non-linear phenomena. The balance between

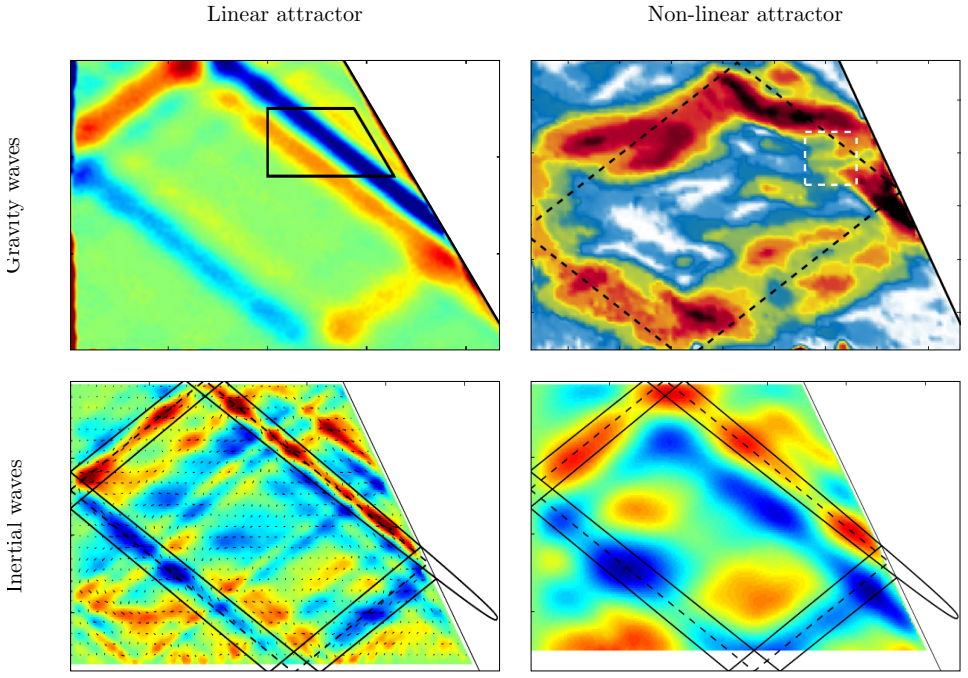

Figure 7. Examples of experimental realization of internal wave attractors. (Top left) Synthetic Schlieren visualization of a linear gravity wave attractor (adapted from [141]). (Top right) Kinetic energy for a non-linear gravity wave attractor (adapted from [92]). (Bottom left) Horizontal velocity field for a linear inertial wave attractor (adapted from [67]). (Bottom right) Horizontal velocity field for a non-linear inertial wave attractor (adapted from [67]).

focusing at the slope and viscous effects can be used to predict the width of the branches of the attractor. Based on experimental results for gravity internal waves [137], this width was predicted to scale as $(\nu/L^2N)^{1/3}$ with L the perimeter of the attractor. This result was checked numerically by Grisouard et al. [138]. For inertial waves, the equivalent scaling factor is $\mathrm{Ek}^{1/3} = (\nu/L^2 f)^{1/3}$, as verified numerically [139, 140].

To illustrate this discussion, a typical linear wave field for both types of attractors is displayed in Figure 7(left). The scaling proposed above was satisfied in the case of a linear inertial wave attractor [67]. For the linear gravity wave attractor, the agreement was less clear [141]. An explanation was further proposed in [142] and validated in [37]. It is related to boundary dissipation effects, whose magnitude is different between the two configurations, due to the size of the tanks. The different tanks were chosen to be adapted to the structure of the waves. For internal gravity waves, the tank had a small thickness compared to the other dimensions and the velocity profiles were measured to be two-dimensional except in the viscous boundary layer near the lateral walls. This layer induces a strong dissipation which is at least ten times larger than the bulk dissipation. This effect is reduced in the case of inertial waves, since the tank is much wider, relatively to the other typical dimensions, and as a consequence, the bulk dissipation dominates. A new scaling law for the size of the branches of the internal wave attractors was then proposed and is in better agreement with experiments [142].

The three-dimensional effects on a wave attractor were then studied for internal gravity waves by Pillet et al. [143] using an extension in the third direction of the quasi-2D experiments performed at ENS de Lyon. These experiments show a trapping of the waves in different 2D planes.

Due to the accumulation of energy in the branches of the attractor, gravity wave attractors and inertial wave attractors are prone to instabilities and in particular triadic resonance instability. Snapshots of the non-linear gravity wave attractor obtained at ENS de Lyon [92, 141, 144] and of the non-linear inertial wave attractor obtained at Paris-Saclay [67] are reproduced in Figure 7. One can still see the geometrical structure, on top of which several other waves have formed. Both studies have shown that the attractor amplitude was reduced and the attractor typical length increased.

Such results were attributed to an energy transfer due to the instability and can be quantified by replacing, in the model for linear attractors, the kinematic viscosity by a turbulent viscosity based on the features of the forced waves [67]. In the non-linear case, strong differences between gravity wave attractors and inertial wave attractors have been observed. An important one is the selectivity of the secondary waves. The feature already mentioned for wave beams (Section 2.2 and Figure 2) is also observed here: indeed, for inertial waves the frequency peaks for the secondary waves are very wide compared to the ones for gravity waves. In addition, there is a clear discrepancy between experimental results for rotating fluids and the 2D numerical simulations [139], while the agreement between experiments and simulations is very good for gravity wave attractors [141]. This weak selectivity in the case of inertial waves can be attributed to the three-dimensional structure of these waves interacting with physical walls, which was clearly neither the case for internal gravity waves [141], nor in the numerical simulations of inertial waves using proper boundary conditions [139]. The second difference concerns the possibility of secondary inertial waves with a non-zero component in the direction perpendicular to the plane of the attractor. This observation, specific to inertial waves and already mentioned for wave beams, could explain the dependence of the secondary waves on Reynolds number, which displays an opposite behavior compared to 2D numerical simulations. Indeed, in the latter case the frequencies ω_1 and ω_2 of the subharmonic waves tend toward $\omega_0/2$ for larger Reynolds number while for experiments they depart from $\omega_0/2$.

4.4. *Axisymmetric Domain: Frustrum*

A second geometry has been widely used to study 3D effects for gravity or inertial wave attractors: the frustrum, i.e. an annulus whose inner cylinder is replaced by a truncated cone. This geometry has been investigated for inertial waves both numerically and experimentally [145–148]. These studies show a wide variety of dynamical systems including linear wave attractors, triadic instability, and emergence of mean flows.

We would like to focus on a similar geometry without the inner cylinder, used in experiments conducted at ENS de Lyon [58]. Using exactly the same experimental setup, rotating fluids and stratified fluids were studied. If the formation of a linear internal wave axisymmetric attractor is similar for both inertial and gravity waves, a major difference is visible for the nonlinear dynamics. Here again, the secondary waves are associated with discrete frequencies for gravity waves contrary to inertial waves for which the frequency range is large, as can be seen in Figure 8 (top, respectively left and right). To explain this behavior, the authors of this study [58] show that the secondary internal waves are the global resonant modes of the tank while the secondary inertial waves are only localized near the center of the tank, as can be seen in the bottom row of Figure 8, left and right respectively. It is explained by the fact that for rotating fluids, standing modes are associated with frequencies larger than the forcing frequency and therefore

not accessible through TRI, resulting only in a local appearance of these secondary waves. The important role of the boundaries is therefore highlighted in the respective non-linear dynamics of gravity and inertial waves. At Paris-Saclay, an experiment to study internal wave turbulence has been designed with inclined panels at the bottom of the tank to inhibit the emergence of wave eigenmodes [149]. In such a configuration, the frequency peaks of the secondary waves excited through TRI are much broader. The frequency spectrum for internal gravity waves becomes therefore closer to the frequency spectrum observed for weakly non-linear inertial waves (Figure 2 right).

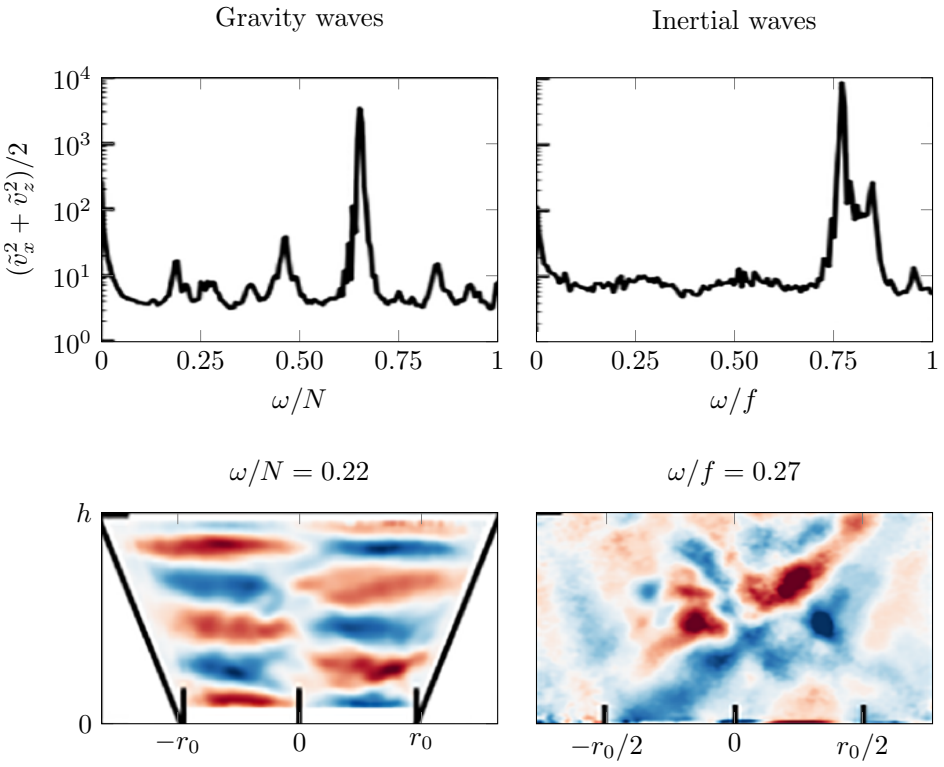

Figure 8. Non-linear behavior of an axisymmetric wave attractor in a frustrum, for gravity waves (left) and inertial waves (right). (Top row) Frequency spectrum. (Bottom row) Snapshots of one of the secondary waves filtered at a given frequency. (Figure adapted from [58]).

Finally, breaking the axisymmetry could induce the trapping of a wave attractor in a particular plane in 3D. This has been recently predicted theoretically and verified numerically [117].

5. Conclusions and Future Directions

In this article, we have discussed several examples of experiments investigating both the linear and non-linear behaviors of internal gravity waves in stratified fluids and of inertial waves in rotating fluids. More specifically, we have focused on the Triadic Resonant Instability (TRI) in various configurations. All these experiments show that, although these waves have a similar dispersion relation, their spatial structure is very important and must be taken into account in

order to accurately predict their linear and non-linear dynamics. In particular, clear differences have been noted in the weakly non-linear regime for different geometries. The main difference is the attraction of energy by discrete frequencies associated to resonances and standing modes in the stratified case. This process seems not to be at play in the rotating case, probably because of the 3D structure of wave field. This observation is of great interest to guide future developments in the study of internal waves.

Recently, efforts have been made to observe, in laboratory experiments, both a weakly non-linear regime of internal gravity wave turbulence in a density stratified fluid [30], and a regime of inertial wave turbulence in a rotating flow [150]. It will be interesting as well to study the similarities and differences in these wave turbulence regimes between gravity and inertial waves.

As mentioned in the introduction, rotating-stratified fluids are ubiquitous in geophysical and astrophysical systems. Laboratory experimental studies combined with theoretical developments and numerical simulations help complement the fundamental understanding of the non-linear behavior of both internal gravity and inertial waves, and therefore help improve the parametrization of (stratified) mixing and other small scale phenomena in climate models. To further assess the role of these waves in atmospheric and oceanic processes, additional features have recently been the focus of a more sustained attention such as the generation of inertial or internal gravity waves due to moving obstacles, the combination of rotation and stratification, the role of a non-linear stratification in density stratified fluids, ice-melting and double diffusive mechanisms, wave-turbulence interaction, wave-mean flow interaction, and the coupling between internal gravity/inertial waves with other type of waves (Lee waves, Kelvin waves, surface waves…). These are important processes that need to be further understood.

Declaration of interests

The authors do not work for, advise, own shares in, or receive funds from any organization that could benefit from this article, and have declared no affiliations other than their research organizations.

References

[1] J. Lighthill, *Waves in fluids*, 3rd edition, Cambridge University Press, 1978.

[2] D. E. Mowbray and B. S. H. Rarity, "The internal wave pattern produced by a sphere moving vertically in a density stratified liquid", *J. Fluid Mech.* **30** (1967), pp. 489–495.

[3] B. R. Sutherland, *Internal gravity waves*, Cambridge University Press, 2010.

[4] H. P. Greenspan, *The Theory of Rotating Fluids*, Cambridge University Press, 1968.

[5] C. Garrett, "Internal Tides and Ocean Mixing", *Science* **301** (2003), no. 5641, pp. 1858–1859.

[6] C. Wunsch and R. Ferrari, "Vertical mixing, energy and the general circulation of the oceans", *Annu. Rev. Fluid Mech.* **36** (2004), pp. 281–314.

[7] J. A. MacKinnon, Z. Zhao, C. B. Whalen, et al., "Climate Process Team on Internal Wave–Driven Ocean Mixing", *Bull. Am. Meteorol. Soc.* **98** (2017), no. 11, pp. 2429–2454.

[8] C. de Lavergne, S. Falahat, G. Madec, F. Roquet, J. Nycander and C. Vic, "Toward global maps of internal tide energy sinks", *Ocean Model.* **137** (2019), pp. 52–75.

[9] F. Pollmann, "Global Characterization of the Ocean's Internal Wave Spectrum", *J. Phys. Oceanogr.* **50** (2020), no. 7, pp. 1871–1891.

[10] U. Achatz, O. Bühler, C. Staquet and W. R. Young, "Multiscale Wave-Turbulence Dynamics in the Atmosphere and Ocean", *Oberwolfach Rep.* **19** (2022), no. 3, pp. 2467–2510.

[11] E. Becker and G. Schmitz, "Climatological Effects of Orography and Land–Sea Heating Contrasts on the Gravity Wave–Driven Circulation of the Mesosphere", *J. Atmos. Sci.* **60** (2003), no. 1, pp. 103–118.

[12] Y.-J. Kim, S. D. Eckermann and H.-Y. Chun, "An overview of the past, present and future of gravity-wave drag parametrization for numerical climate and weather prediction models", *Atmosphere-Ocean* **41** (2003), no. 1, pp. 65–98.

[13] A. de la Cámara, F. Lott and M. Abalos, "Climatology of the middle atmosphere in LMDz: Impact of source-related parameterizations of gravity wave drag", *Journal of Advances in Modeling Earth Systems* **8** (2016), no. 4, pp. 1507–1525.
[14] L. A. Holt, F. Lott, R. R. Garcia, et al., "An evaluation of tropical waves and wave forcing of the QBO in the QBOi models", *Q. J. R. Meteorol. Soc.* **148** (2022), no. 744, pp. 1541–1567.
[15] R. R. Kerswell and W. V. R. Malkus, "Tidal instability as the source for Io's magnetic signature", *Geophys. Res. Lett.* **25** (1998), no. 5, pp. 603–606.
[16] G. I. Ogilvie and D. N. C. Lin, "Tidal Dissipation in Rotating Giant Planets", *Astrophys. J.* **610** (2004), no. 1, pp. 477–509.
[17] T. Sidery, N. Andersson and G. L. Comer, "Waves and instabilities in dissipative rotating superfluid neutron stars", *Mon. Not. Roy. Astron. Soc.* **385** (2008), no. 1, pp. 335–348.
[18] M. Le Bars, D. Cébron and P. Le Gal, "Flows Driven by Libration, Precession, and Tides", *Ann. Rev. Fluid Mech.* **47** (2015), pp. 163–193.
[19] M. Bouffard, B. Favier, D. Lecoanet and M. Le Bars, "Internal gravity waves in a stratified layer atop a convecting liquid core in a non-rotating spherical shell", *Geophys. J. Int.* **228** (2021), no. 1, pp. 337–354.
[20] S. Dauxois T. rand Joubaud, P. Odier and A. Venaille, "Instabilities of Internal Gravity Wave Beams", *Ann. Rev. of Fluid Mech.* **50** (2018), pp. 131–156.
[21] C. Staquet and J. Sommeria, "Internal gravity waves: From instabilities to turbulence", *Annu. Rev. Fluid Mech.* **34** (2002), pp. 559–593.
[22] G. Veronis, "The analogy between rotating and stratified fluids", *Ann. Rev. Fluid Mech.* **2** (1970), pp. 36–67.
[23] S. Medvedev and V. Zeitlin, "Parallels between stratification and rotation in hydrodynamics, and between both of them and external magnetic field in magnetohydrodynamics, with applications to nonlinear waves", in *IUTAM Symposium on Turbulence in the Atmosphere and Oceans* (D. Dritschel, ed.), Springer, 2010, pp. 27–37.
[24] P. Maurer, *Approche expérimentale de la dynamique non-linéaire d'ondes internes en rotation*, PhD thesis, Université de Lyon, France, 2017.
[25] D. E. Mowbray and B. S. H. Rarity, "A theoretical and experimental investigation of the phase configuration of internal waves of small amplitude in a density stratified liquid", *J. Fluid Mech.* **28** (1967), no. 1, pp. 1–16.
[26] T. Peacock and A. Tabaei, "Visualization of nonlinear effects in reflecting internal wave beams", *Phys. Fluids* **17** (2005), no. 6, article no. 061702.
[27] G. Brethouwer, P. Billant, E. Lindborg and J.-M. Chomaz, "Scaling analysis and simulation of strongly stratified turbulent flows", *J. Fluid Mech.* **585** (2007), pp. 343–368.
[28] G. N. Ivey, K. B. Winters and J. R. Koseff, "Density stratification, turbulence, but how much mixing?", *Annu. Rev. Fluid Mech.* **40** (2008), pp. 169–184.
[29] C. P. Caulfield, "Layering, Instabilities, and Mixing in Turbulent Stratified Flows", *Ann. Rev. Fluid Mech.* **53** (2021), no. 1, pp. 113–145.
[30] P.-P. Cortet and L. Lanchon, "Turbulence of internal gravity waves in the laboratory", *C. R. Phys* (2024). online first.
[31] S. Boury, *Energy and Buoyancy Transport by Inertia-Gravity Waves in Non-Linear Stratifications. Application to the Ocean*, PhD thesis, Université de Lyon, Lyon, France, 2020.
[32] D. W. Moore and P. G. Saffman, "The structure of free vertical shear layers in a rotating fluid and the motion produced by a slowly rising body", *Philos. Trans. R. Soc. Lond., Ser. A* **264** (1969), no. 1156, pp. 597–634.
[33] N. H. Thomas and T. N. Stevenson, "A similarity solution for viscous internal waves", *J. Fluid Mech.* **54** (1972), no. 3, pp. 495–506.
[34] M. Nikurashin and R. Ferrari, "Radiation and Dissipation of Internal Waves Generated by Geostrophic Motions Impinging on Small-Scale Topography: Theory", *J. Phys. Oceanogr.* **40** (2010), no. 5, pp. 1055–1074.
[35] A. M. M. Manders, J. J. Duistermaat and L. R. M. Maas, "Wave attractors in a smooth convex enclosed geometry", *Phys. D: Nonlinear Phenom.* **186** (2003), no. 3-4, pp. 109–132.
[36] P.-Y. Passaggia, P. Meunier and S. Le Dizès, "Response of a stratified boundary layer on a tilted wall to surface undulations", *J. Fluid Mech.* **751** (2014), pp. 663–684.
[37] G. Davis, T. Dauxois, T. Jamin and S. Joubaud, "Energy budget in internal wave attractor experiments", *J. Fluid Mech.* **880** (2019), pp. 743–763.
[38] E. Horne, F. Beckebanze, D. Micard, P. Odier, L. R. M. Maas and S. Joubaud, "Particle transport induced by internal wave beam streaming in lateral boundary layers", *J. Fluid Mech.* **870** (2019), pp. 848–869.
[39] S. Le Dizès, "Reflection of oscillating internal shear layers: nonlinear corrections", *J. Fluid Mech.* **899** (2020), article no. A21.
[40] G. Bordes, F. Moisy, T. Dauxois and P.-P. Cortet, "Experimental evidence of a triadic resonance of plane inertial waves in a rotating fluid", *Phys. Fluids* **24** (2012), no. 1, article no. 014105.
[41] A. Renaud and A. Venaille, "Boundary streaming by internal waves", *J. Fluid Mech.* **858** (2019), pp. 71–90.

[42] M. A. Calkins, J. Noir, J. D. Eldredge and J. M. Aurnou, "Axisymmetric simulations of libration-driven fluid dynamics in a spherical shell geometry", *Phys. Fluids* **22** (2010), no. 8, article no. 086602.
[43] A. Tilgner, "Kinematic dynamos with precession driven flow in a sphere", *Geophys. Astro. Fluid* **101** (2007), no. 1, pp. 1–9.
[44] C. Morize, M. Le Bars, P. Le Gal and A. Tilgner, "Experimental Determination of Zonal Winds Driven by Tides", *Phys. Rev. Lett.* **104** (2010), no. 21, article no. 214501.
[45] Y. Onuki, S. Joubaud and T. Dauxois, "Simulating turbulent mixing caused by local instability of internal gravity waves", *J. Fluid Mech.* **915** (2021), article no. A77.
[46] C. B. Whalen, C. de Lavergne, A. C. Naveira Garabato, J. M. Klymak, J. A. MacKinnon and K. L. Sheen, "Internal wave-driven mixing: governing processes and consequences for climate", *Nat. Rev. Earth Environ.* **1** (2020), no. 11, pp. 606–621.
[47] Y. Dossmann, B. Bourget, C. Brouzet, T. Dauxois, S. Joubaud and P. Odier, "Mixing by internal waves quantified using combined PIV/PLIF technique", *Exp. Fluids* **57** (2016), no. 8, article no. 132.
[48] Y. Dossmann, F. Pollet, P. Odier and T. Dauxois, "Mixing and Formation of Layers by Internal Wave Forcing", *J. Geophys. Res. Oceans* **122** (2017), no. 12, pp. 9906–9917.
[49] J. M. H. Fortuin, "Theory and application of two supplementary methods of constructing density gradient columns", *J. Polym. Sci.* **44** (1960), no. 144, pp. 505–515.
[50] G. Oster and M. Yamamoto, "Density Gradient Techniques", *Chem. Rev.* **63** (1963), no. 3, pp. 257–268.
[51] D. F. Hill, "General density gradients in general domains: the "two-tank" method revisited", *Exp. Fluids* **32** (2002), no. 4, pp. 434–440.
[52] K. D. Stewart, C. J. Shakespeare, Y. Dossmann and A. M. Hogg, "A simple technique for developing and visualising stratified fluid dynamics: the hot double-bucket", *Exp. Fluids* **62** (2021), no. 5, article no. 103.
[53] S. B. Dalziel, G. O. Hughes and B. R. Sutherland, "Whole-field density measurements by 'synthetic schlieren'", *Exp. Fluids* **28** (2000), no. 4, pp. 322–335.
[54] A. M. van Oers, R. de Kat and L. R. M. Maas, "Whole-field density measurements by digital image correlation", *Exp. Fluids* **64** (2023), no. 11, p. 175.
[55] D. Benielli and J. Sommeria, "Excitation of internal waves and stratified turbulence by parametric instability", *Dynam. Atmos. Oceans* **23** (1996), no. 1-4, pp. 335–343. 4th International Symposium on Stratified Flows, Grenoble, France, Jun 29 - Jul 02, 1994.
[56] J. Noir, D. Cébron, M. Le Bars, A. Sauret and J. M. Aurnou, "Experimental study of libration-driven zonal flows in non-axisymmetric containers", *Phys. Earth Planet. Inter.* **204** (2012), pp. 1–10.
[57] C. Savaro, A. Campagne, M. C. Linares, et al., "Generation of weakly nonlinear turbulence of internal gravity waves in the Coriolis facility", *Phys. Rev. Fluids* **5** (2020), no. 7, article no. 073801.
[58] C. Pacary, T. Dauxois, E. Ermanyuk, P. Metz, M. Moulin and S. Joubaud, "Observation of inertia-gravity wave attractors in an axisymmetric enclosed basin", *Phys. Rev. Fluids* **8** (2023), no. 10, article no. 104802.
[59] T. Dauxois, A. Didier and E. Falcon, "Observation of near-critical reflection of internal waves in a stably stratified fluid", *Phys. Fluids* **16** (2004), no. 6, pp. 1936–1941.
[60] B. Voisin, E. V. Ermanyuk and J.-B. Flór, "Internal wave generation by oscillation of a sphere, with application to internal tides", *J. Fluid Mech.* **666** (2011), pp. 308–357.
[61] M. Duran-Matute, J.-B. Flór, F. S. Godeferd and C. Jause-Labert, "Turbulence and columnar vortex formation through inertial-wave focusing", *Phys. Rev. E* **87** (2013), no. 4, article no. 041001.
[62] E. Monsalve, M. Brunet, B. Gallet and P.-P. Cortet, "Quantitative experimental observation of weak inertial-wave turbulence", *Phys. Rev. Lett.* **125** (2020), no. 25, article no. 254502.
[63] L. Gostiaux and T. Dauxois, "Laboratory experiments on the generation of internal tidal beams over steep slopes", *Phys. Fluids* **19** (2007), no. 2, article no. 028102.
[64] M. M. Scase and S. B. Dalziel, "Internal wave fields generated by a translating body in a stratified fluid: an experimental comparison", *J. Fluid Mech.* **564** (2006), pp. 305–331.
[65] L. Gostiaux, H. Didelle, S. Mercier and T. Dauxois, "A novel internal waves generator", *Exp. Fluids* **42** (2007), no. 1, pp. 123–130.
[66] T. E. Dobra, A. G. W. Lawrie and S. B. Dalziel, "The magic carpet: an arbitrary spectrum wave maker for internal waves", *Exp. Fluids* **60** (2019), pp. 1–14.
[67] M. Brunet, T. Dauxois and P.-P. Cortet, "Linear and nonlinear regimes of an inertial wave attractor", *Phys. Rev. Fluids* **4** (2019), no. 3, article no. 034801.
[68] P. Husseini, D. Varma, T. Dauxois, S. Joubaud, P. Odier and M. Mathur, "Experimental study on superharmonic wave generation by resonant interaction between internal wave modes", *Phys. Rev. Fluids* **5** (2020), no. 7, article no. 074804.
[69] P. Maurer, S. J. Ghaemsaidi, S. Joubaud, T. Peacock and P. Odier, "An axisymmetric inertia-gravity wave generator", *Exp. Fluids* **58** (2017), no. 10, article no. 143.

[70] W. V. R. Malkus, "An experimental study of global instabilities due to the tidal (elliptical) distortion of a rotating elastic cylinder", *Geophys. Astrophys. Fluid Dyn.* **48** (1989), no. 1-3, pp. 123–134.

[71] B. Favier, A. Grannan, T. Le Reun, J. Aurnou and M. Le Bars, "The turbulent response to tidal and libration forcing", in *Astro Fluid: An International Conference in Memory of Professor Jean-Paul Zahn's Great Scientific Achievements*, EDP Sciences, 2019, pp. 51–58.

[72] J. R. Munroe and B. R. Sutherland, "Generation of internal waves by sheared turbulence: experiments", *Environ. Fluid Mech.* **8** (2008), pp. 527–534.

[73] V. Dorel, P. Le Gal and M. Le Bars, "Experimental study of the penetrative convection in gases", *Phys. Rev. Fluids* **8** (2023), article no. 103501.

[74] P. Flandrin, *Time-Frequency/Time-Scale Analysis, Time-Frequency Toolbox for Matlab©*, Academic Press, San Diego, 1999.

[75] M. J. Mercier, N. B. Garnier and T. Dauxois, "Reflection and diffraction of internal waves analyzed with the Hilbert transform", *Phys. Fluids* **20** (2008), no. 8, article no. 086601.

[76] M. Mathur and T. Peacock, "Internal wave interferometry", *Phys. Rev. Lett.* **104** (2010), no. 11, article no. 118501.

[77] R. Supekar and T. Peacock, "Interference and transmission of spatiotemporally locally forced internal waves in non-uniform stratifications", *J. Fluid Mech.* **866** (2019), pp. 350–368.

[78] S. Boury, T. Peacock and P. Odier, "Excitation and resonant enhancement of axisymmetric internal wave modes", *Phys. Rev. Fluids* **4** (2019), no. 3, article no. 034802.

[79] E. Horne, J. Schmitt, N. Pustelnik, S. Joubaud and P. Odier, "Variational Mode Decomposition for estimating critical reflected internal wave in stratified fluid", *Exp. Fluids* **62** (2021), article no. 110.

[80] S. Boury, B. R. Sutherland, S. Joubaud, T. Peacock and P. Odier, "Axisymmetric internal wave tunneling", 2024.

[81] K. M. Grayson, S. B. Dalziel and A. G. W. Lawrie, "The long view of triadic resonance instability in finite-width internal gravity wave beams", *J. Fluid Mech.* **953** (2022), article no. A22.

[82] J. Hazewinkel, S. B. Dalziel, A. Doelman and L. R. M. Maas, "Tracer transport by internal wave beams", 2010.

[83] B. Bourget, T. Dauxois, S. Joubaud and P. Odier, "Experimental study of parametric subharmonic instability for internal plane waves", *J. Fluid Mech.* **723** (2013), pp. 1–20.

[84] B. Bourget, H. Scolan, T. Dauxois, M. Le Bars, P. Odier and S. Joubaud, "Finite-size effects in parametric subharmonic instability", *J. Fluid Mech.* **759** (2014), pp. 739–750.

[85] G. Bordes, *Interactions non-linéaires d'ondes et tourbillons en milieu stratifié ou tournant*, PhD thesis, Université de Lyon, Lyon, France, 2012.

[86] R. E. Davis and A. Acrivos, "The stability of oscillatory internal waves", *J. Fluid Mech.* **30** (1967), no. 4, pp. 723–736.

[87] A. D. McEwan and R. M. Robinson, "Parametric-Instability of Internal Gravity-Waves", *J. Fluid Mech.* **67** (1975), no. FEB25, pp. 667–687.

[88] D. Benielli and J. Sommeria, "Excitation and breaking of internal gravity waves by parametric instability", *J. Fluid Mech.* **374** (1998), pp. 117–144.

[89] S. Joubaud, J. Munroe, P. Odier and T. Dauxois, "Experimental parametric subharmonic instability in stratified fluids", *Phys. Fluids* **24** (2012), no. 4, article no. 041703.

[90] J. A. MacKinnon, M. H. Alford, O. Sun, R. Pinkel, Z. Zhao and J. Klymak, "Parametric subharmonic instability of the internal tide at 29 N", *J. Phys. Oceanogr.* **43** (2013), no. 1, pp. 17–28.

[91] Q. Hu et al., "Parametric Subharmonic Instability of Diurnal Internal Tides in the Abyssal South China Sea", *J. Phys. Oceanogr.* **53** (2023), no. 1, pp. 195–213.

[92] C. Brouzet, E. V. Ermanyuk, S. Joubaud, I. Sibgatullin and T. Dauxois, "Energy cascade in internal-wave attractors", *Europhysics Letters* **113** (2016), no. 4, article no. 44001.

[93] P. Maurer, S. Joubaud and P. Odier, "Generation and stability of inertia-gravity waves", *J. Fluid Mech.* **808** (2016), pp. 539–561.

[94] D. O. Mora, E. Monsalve, M. Brunet, T. Dauxois and P.-P. Cortet, "Three-dimensionality of the triadic resonance instability of a plane inertial wave", *Phys. Rev. Fluids* **6** (2021), no. 7, article no. 074801.

[95] S. J. Ghaemsaidi and M. Mathur, "Three-dimensional small-scale instabilities of plane internal gravity waves", *J. Fluid Mech.* **863** (2019), pp. 702–729.

[96] K. N. Kumar, T. K. Ramkumar and M. Krishnaiah, "MST radar observation of inertia-gravity waves generated from tropical cyclones", *J. Atmos. Sol.-Terr. Phys.* **73** (2011), pp. 1890–1906.

[97] W. H. Schubert, J. J. Hack, P. L. Silva Dias and S. R. Fulton, "Geostrophic adjustment in an axisymmetric vortex", *J. Atmos. Sol.-Terr. Phys.* **37** (1980), pp. 1464–1484.

[98] T. N. Stevenson, "Axisymmetric Internal Waves Generated by a Travelling Oscillating Body", *J. Fluid Mech.* **35** (1969), pp. 219–224.

[99] M. R. Flynn, K. Onu and B. R. Sutherland, "Internal wave excitation by a vertically oscillating sphere", *J. Fluid Mech.* **494** (2003), pp. 65–93.

[100] J. K. Ansong and B. R. Sutherland, "Internal gravity waves generated by convective plumes", *J. Fluid Mech.* **648** (2010), pp. 405–434.
[101] S. Boury, P. Maurer, S. Joubaud, T. Peacock and P. Odier, "Triadic resonant instability in confined and unconfined axisymmetric geometries", *J. Fluid Mech.* **957** (2023), article no. A20.
[102] E. V. Ermanyuk, J.-B. Flór and B. Voisin, "Spatial Structure of First and Higher Harmonic Internal Waves from a Horizontally Oscillating Sphere", *J. Fluid Mech.* **671** (2011), pp. 364–383.
[103] S. J. Ghaemsaidi, H. V. Dosser, L. Rainville and T. Peacock, "The impact of multiple layering on internal wave transmission", *J. Fluid Mech.* **789** (2016), pp. 617–629.
[104] T. Peacock and P. Weidman, "The Effect of Rotation on Conical Wave Beams in a Stratified Fluid", *Exp. Fluids* **39** (2005), pp. 32–37.
[105] E. V. Ermanyuk, N. D. Shmakova and J.-B. Flór, "Internal Wave Focusing by a Horizontally Oscillating Torus", *J. Fluid Mech.* **813** (2017), pp. 695–715.
[106] D. Guimbard, *L'instabilité elliptique en milieu stratifié tournant*, PhD thesis, Université du Sud Toulon Var, France, 2008.
[107] D. Guimbard, S. Le Dizès, M. Le Bars, P. Le Gal and S. Leblanc, "Elliptic instability of a stratified fluid in a rotating cylinder", *J. Fluid Mech.* **660** (2010), pp. 240–257.
[108] S. Boury, T. Peacock and P. Odier, "Experimental generation of axisymmetric internal wave super-harmonics", *Phys. Rev. Fluids* **6** (2021), no. 6, article no. 064801.
[109] N. D. Shmakova and J.-B. Flór, "Nonlinear aspects of focusing internal waves", *J. Fluid Mech.* **862** (2019), article no. R4.
[110] G. Michel, "Three-wave interactions among surface gravity waves in a cylindrical container", *Phys. Rev. Fluids* **4** (2019), article no. 012801.
[111] L. E. Baker and B. R. Sutherland, "The evolution of superharmonics excited by internal tides in non-uniform stratification", *J. Fluid Mech.* **891** (2020), article no. R1.
[112] T. Dauxois and W. R. Young, "Near-critical reflection of internal waves", *J. Fluid Mech.* **390** (1999), pp. 271–295.
[113] O. M. Phillips, "Energy Transfer in Rotating Fluids by Reflection of Inertial Waves", *The Physics of Fluids* **6** (1963), no. 4, pp. 513–520.
[114] C. C. Eriksen, "Observations of internal wave reflection off sloping bottoms", *J. Geophys. Res. Oceans* **87** (1982), no. C1, pp. 525–538.
[115] A. M. M. Manders and L. R. M. Maas, "On the three-dimensional structure of the inertial wave field in a rectangular basin with one sloping boundary", *Fluid Dyn. Res.* **35** (2004), no. 1, pp. 1–21.
[116] G. Pillet, L. R. M. Maas and T. Dauxois, "Internal wave attractors in 3D geometries : A dynamical systems approach", *Eur. J. Mech. B Fluids* **77** (2019), pp. 1–16.
[117] B. Favier and S. Le Dizès, "Inertial wave super-attractor in a truncated elliptic cone", *J. Fluid Mech.* **980** (2024), article no. A6.
[118] L. R. M. Maas and F. P. A. Lam, "Geometric focusing of internal waves", *J. Fluid Mech.* **300** (1995), pp. 1–41.
[119] J. Bajars, J. Frank and L. R. M. Maas, "On the appearance of internal wave attractors due to an initial or parametrically excited disturbance", *J. Fluid Mech.* **714** (2013), pp. 283–311.
[120] Y. Colin de Verdière and L. Saint-Raymond, "Attractors for Two-Dimensional Waves with Homogeneous Hamiltonians of Degree 0", *Commun. Pure Appl. Math.* **73** (2020), no. 2, pp. 421–462.
[121] Z. V. Makridin, A. K. Khe, I. N. Sibgatullin and E. V. Ermanyuk, "Forced internal wave attractors: Linear inviscid theory", *Phys. Rev. Fluids* **8** (2023), no. 8, article no. 084801.
[122] I. N. Sibgatullin and E. V. Ermanyuk, "Internal and Inertial Wave Attractors: A Review", *J. Appl. Mech. Tech. Phys.* **60** (2019), no. 2, pp. 284–302.
[123] M. E. Stern, "Trapping of low frequency oscillations in an equatorial boundary layer", *Tellus* **15** (1963), pp. 246–250.
[124] F. P. Bretherton, "Low frequency oscillations trapped near the equator", *Tellus* **16** (1964), no. 2, pp. 181–185.
[125] K. Stewartson, "On trapped oscillations of a rotating fluid in a thin spherical shell II", *Tellus* **24** (1972), pp. 283–287.
[126] M. Rieutord and L. Valdettaro, "Inertial waves in a rotating spherical shell", *J. Fluid Mech.* **341** (1997), pp. 77–99.
[127] M. Rieutord, B. Georgeot and L. Valdettaro, "Wave attractors in rotating fluids: a paradigm for ill-posed Cauchy problems", *Phys. Rev. Lett.* **435** (2001), pp. 103–144.
[128] M. Rieutord and L. Valdettaro, "Viscous dissipation by tidally forced inertial modes in a rotating spherical shell", *J. Fluid Mech.* **643** (2010), pp. 363–394.
[129] A. Rabitti and L. R. M. Maas, "Equatorial wave attractors and inertial oscillations", *J. Fluid Mech.* **729** (2013), pp. 445–470.
[130] B. Favier, A. J. Barker, C. Baruteau and G. I. Ogilvie, "Non-linear evolution of tidally forced inertial waves in rotating fluid bodies", *Mon. Not. R. Astron. Soc.* **439** (2014), pp. 845–860.

[131] J. He, B. Favier, M. Rieutord and S. Le Dizès, "Internal shear layers in librating spherical shells: the case of attractors", *J. Fluid Mech.* **974** (2023), article no. A3.

[132] A. M. M. Manders, L. R. M. Maas and T. Gerkema, "Observations of internal tides in the Mozambique Channel", *J. Geophys. Res. Oceans* **109** (2004), no. C12.

[133] W. Tang and T. Peacock, "Lagrangian coherent structures and internal wave attractors", *Chaos* **20** (2010), no. 1, article no. 017508.

[134] G. Wang, Q. Zheng, M. Lin, D. Dai and F. Qiao, "Three dimensional simulation of internal wave attractors in the Luzon Strait", *Acta Oceanologica Sinica* **34** (2015), no. 11, pp. 14–21.

[135] L. R. M. Maas, D. Benielli, J. Sommeria and F. P. A. Lam, "Observations of an internal wave attractor in a confined stably stratified fluid", *Nature* **388** (1997), pp. 557–561.

[136] L. R. M. Maas, "Wave focusing and ensuing mean flow due to symmetry breaking in rotating fluids", *J. Fluid Mech.* **437** (2001), pp. 13–28.

[137] J. Hazewinkel, P. van Breevoort, S. Dalziel and L. R. M. Maas, "Observations on the wavenumber spectrum and evolution of an internal wave attractor", *J. Fluid Mech.* **598** (2008), pp. 373–382.

[138] N. Grisouard, C. Staquet and I. Pairaud, "Numerical simulation of a two-dimensional internal wave attractor", *J. Fluid Mech.* **614** (2008), pp. 1–14.

[139] L. Jouve and G. I. Ogilvie, "Direct numerical simulations of an inertial wave attractor in linear and nonlinear regime", *J. Fluid Mech.* **745** (2014), pp. 223–250.

[140] K. Wu, B. D. Welfert and J. M. Lopez, "Inertial wave attractors in librating cuboids", *J. Fluid Mech.* **973** (2023), article no. A20.

[141] C. Brouzet, I. N. Sibgatullin, H. Scolan, E. V. Ermanyuk and T. Dauxois, "Internal wave attractors examined using laboratory experiments and 3D numerical simulations", *J. Fluid Mech.* **793** (2016), pp. 109–131.

[142] F. Beckebanze, C. Brouzet, I. N. Sibgatullin and L. R. M. Maas, "Damping of quasi-two-dimensional internal wave attractors by rigid-wall friction", *J. Fluid Mech.* **841** (2018), pp. 614–635.

[143] G. Pillet, E. V. Ermanyuk, L. R. M. Maas, I. N. Sibgatullin and T. Dauxois, "Internal wave attractors in three-dimensional geometries: trapping by oblique reflection", *J. Fluid Mech.* **845** (2018), pp. 203–225.

[144] C. Brouzet, E. Ermanyuk, S. Joubaud, G. Pillet and T. Dauxois, "Internal wave attractors: different scenarios of instability", *J. Fluid Mech.* **811** (2017), pp. 544–568.

[145] A. Swart, A. Manders, U. Harlander and L. R. M. Maas, "Experimental observation of strong mixing due to internal wave focusing over sloping terrain", *Dynam. Atmos. Oceans* **50** (2010), no. 1, pp. 16–34.

[146] M. Klein, T. Seelig, M. V. Kurgansky, et al., "Inertial wave excitation and focusing in a liquid bounded by a frustum and a cylinder", *J. Fluid Mech.* **751** (2014), pp. 255–297.

[147] I. Sibgatullin, X. Xu, A. Tretyakov and E. Ermanyuk, "Influence of geometry on energy flow and instability in inertial wave attractors for rotating annular frustum", *AIP Conf. Proc.* **2116** (2019), no. 1, article no. 030034.

[148] S. Boury, I. Sibgatullin, E. Ermanyuk, et al., "Vortex cluster arising from an axisymmetric inertial wave attractor", *J. Fluid Mech.* **926** (2021), article no. A12.

[149] N. Lanchon, D. O. Mora, E. Monsalve and P.-P. Cortet, "Internal wave turbulence in a stratified fluid with and without eigenmodes of the experimental domain", *Phys. Rev. Fluids* **8** (2023), no. 5, article no. 054802.

[150] S. Galtier, "Inertial Wave Turbulence", in *Physics of Wave Turbulence*, Cambridge University Press, 2022, pp. 155–178.